

# Theoretical Study of Time-Resolved Fluorescence Anisotropy from Coupled Chromophore Pairs

Alexander Matro<sup>†</sup> and Jeffrey A. Cina

*Department of Chemistry and The James Franck Institute, The University of Chicago, Chicago,*

*IL 60637*

( )

In press, *J. Phys. Chem.* (S. A. Rice issue)

## Abstract

Calculations of time-resolved fluorescence anisotropy from a pair of chromophores coupled by an excitation transfer interaction are presented. For the purpose of investigating the effects of nuclear motion on the energy transfer and anisotropy, an illustrative model is developed that provides each chromophore with a single intramolecular vibrational mode. Account is taken of non-instantaneous excitation and time- and frequency-resolved detection. Effects of excitation pulse duration, detection window duration and frequency resolution, and excitation transfer coupling strength on the time-resolved anisotropy are examined in detail. Effects of vibrational relaxation and dephasing are also examined using a simplified Redfield description of the effects of coupling to a thermal bath.

<sup>†</sup>Present Address: Department of Chemistry, University of Rhode Island, Kingston, Rhode Island 02881

## 1. INTRODUCTION

The process of electronic excitation transfer among chromophores has been widely studied. [1] In photosynthetic antenna systems, efficient excitation transfer among pigment molecules is responsible for greatly enhancing the availability of energy for photosynthesis. [2] Studies of electronic excitation transfer among impurities in molecular crystals have examined the effects of the coupling between electronic and vibrational excitations. [3] With the availability of ultrafast lasers it is now possible to study excitation transfer processes occurring on picosecond and sub-picosecond timescales, enabling researchers to directly observe some of the fastest excitation transfer processes taking place in photosynthetic antenna systems and elsewhere. Generally speaking, the efficiency of excitation transfer depends on the proximity of chromophores, their spectral properties, their relative orientations, and their interactions with the surrounding medium. When the chromophores coupled by excitation transfer differ in the orientation of their transition dipole moments, fluorescence (or stimulated emission or ground state bleaching) can occur with polarization and frequency different from those of the exciting field. For this reason, measurement of some variety of time-resolved anisotropy can often provide information on electronic energy transport. Two experimental methods employing linearly polarized light, pump-probe and fluorescence upconversion, have been used recently to obtain time-resolved anisotropies. The time-resolved fluorescence upconversion signal is obtained by combining the fluorescence induced by a laser pulse with a delayed gate pulse in a non-linear crystal and collecting the sum-frequency signal as a function of the delay time between excitation and gate pulses. By setting the polarization of the electric field of the excitation pulse parallel or perpendicular to that of the gate pulse, parallel ( $S_{\parallel}(t)$ ) or perpendicular ( $S_{\perp}(t)$ ) components of the transient fluorescence are measured. The anisotropy is then calculated according to the expression

$$R(t) = \frac{S_{\parallel}(t) - S_{\perp}(t)}{S_{\parallel}(t) + 2S_{\perp}(t)}. \quad (1)$$

In pump-probe anisotropy measurements, the signal is the relative transmittance of a delayed probe pulse. Here the pump pulse is polarized parallel or perpendicular to a probe pulse,

which passes through the sample, rather than to a gate pulse, which does not.

Using fluorescence upconversion, Xie *et al.* [4] recently measured time-resolved anisotropy from Allophycocyanin (APC) and C-Phycocyanin (C-PC), the pigment-protein complexes isolated from antenna systems of photosynthetic cyanobacteria. The structure of the trimeric form of C-PC has been investigated with x-ray crystallography, [5] which revealed that chromophores on adjacent monomers are located within  $\sim 2$  nm of one another, whereas inter-chromophore distances within individual monomers are  $\sim 5$  nm. Xie *et al.* observed sub-picosecond decays in the fluorescence anisotropy in APC and C-PC. Earlier experiments by Beck and Sauer [6] employing pump-probe techniques showed that anisotropy in APC monomers fails to exhibit sub-picosecond time dependence. Xie and co-workers attributed the ultrafast decay in trimeric APC and C-PC to energy transfer between chromophores on adjacent monomers. Recent femtosecond pump-probe experiments by Gillbro *et al.* [7] have also observed a sub-picosecond anisotropy decay in C-PC. Rapid anisotropy decays have also been observed by Kim *et al.* [8] and Zhu *et al.* [9] in bichromophoric compounds 9,9'-bifluorene and 2,2'-binaphthyl in solution using fluorescence upconversion [8] and pump-probe techniques. [9,10]

Xie and co-workers [4] made an additional interesting observation that the asymptotic value of the anisotropy following the ultrafast decay was sensitive to the excitation and detection conditions used. In both C-PC and APC, excitation at the approximate peak of the APC and C-PC absorption spectra resulted in significantly lower long time values of the anisotropy than excitation closer to the red edge of the absorption spectrum, suggesting that a larger fraction of excited chromophores transfer their excitation prior to fluorescence in the former case.

Time-resolved anisotropy can also be a measure of coherence among exciton states, as shown in a recent experimental study by Galli *et al.* [11], where an initial anisotropy of 0.7 was found in a pump-probe experiment on magnesium tetraphenylporphyrin in solution. This finding supported earlier theoretical work by Wynne and Hochstrasser [12] in which an initial anisotropy of 0.7 was predicted in a molecule having two degenerate electronic transi-

tions originating from a single ground state, with perpendicular transition dipole moments. Wynne and Hochstrasser [12] and Knox and Gülen [13] have also examined the case of two chromophores with a fixed relative angle between their transition dipole moments, showing that such a system can exhibit an anisotropy larger than 0.4, the initial anisotropy observed in a collection of randomly oriented single chromophores.

Electronic energy transfer received a thorough theoretical treatment by Förster [14], who examined the effects of coupling strength, site energy differences, and details of potential energy surfaces and nuclear vibrations on excitation transfer between a pair of chromophores. Later work by Rackovsky and Silbey focused on the effects of exciton-phonon interactions on excitation transfer among chromophores embedded in a solid. [3] A theoretical study by Rahman, Knox and Kenkre [15] investigated the fluorescence depolarization resulting from electronic energy transfer, pointing out that electronically off-diagonal density matrix elements need to be included in order to correctly calculate the polarized fluorescence signal.

Previous theoretical treatments of time-resolved polarized emission from chromophore pairs [9,13,15] (and single molecules with degenerate electronic transitions [12]) have neglected the nuclear degrees of freedom, treating each chromophore as an electronic 2-level system. Because femtosecond pulses can launch vibrational wave packets in both ground and excited electronic states [16], the effects of vibrational motion should be included in the calculation of time-resolved signals. In terms of the eigenstates of the uncoupled chromophore pair expressed as products of eigenstates of individual chromophores, we can say that Franck-Condon factors and energy level spacings between vibronic states modify the effect of a given electronic energy transfer interaction. [14] In addition, different sets of states can be selected depending on excitation and detection center frequencies and bandwidths.

In connection to the general issue of simultaneous vibrational coherence and electronic energy transfer, it should be pointed out that vibrational quantum beats [17] and exciton dynamics [18] have been observed in ultrafast pump-probe anisotropy measurements on the light-harvesting complexes of *Rhodobacter sphaeroides* at 4 K. While an interesting argument was advanced [18] for the observed spectral and polarization dynamics, no attempt

was reported to incorporate both nuclear and electronic dynamics in a single model. The light-harvesting complex LH1 of *Rhodobacter sphaeroides* has also been the subject of room temperature femtosecond fluorescence anisotropy measurements. [19]

Here we investigate a model chromophore pair interacting with a simple detection apparatus in order to explore the roles that molecular parameters and the characteristics of the excitation and detection processes play on the calculated time-resolved fluorescence anisotropy. In order to study the effects of vibrational motion on the time-resolved anisotropy, each chromophore is considered to have a single intramolecular vibrational mode. This model is presented in Section 2.

An analytic treatment of a chromophore pair having a minimal number of states, presented in Section 3, highlights an important way that chromophore vibrational structure can influence the initial anisotropy. Recapitulating the argument of Knox and Gülen [13,15] it is first illustrated how interference in emission from singly excited states with different chromophores excited can lead to an initial anisotropy greater than 0.4. The excited states must, of course, emit to the same vibronic level of the electronic ground state in order for interference to occur. It is pointed out that some vibronic levels are accessible from singly excited states having only one specific chromophore excited, and that emission into vibronic levels that reveal the identity of the excited chromophore tend to suppress high initial values of the anisotropy.

Having included an intramolecular vibrational mode on each chromophore, we are able to examine the roles of simultaneous coherent vibrational and electronic motion induced by the ultrashort excitation laser pulse on the anisotropy. Section 4 details these numerical calculations. We first choose the parameters of the chromophore pair and the excitation and detection processes to correspond as closely as possible to the known parameters in experiments by Xie *et al.* [4] and compare our findings with their experimental results. Then we investigate the effects on the anisotropy of varying the molecular and detector parameters, such as the strength of the excitation transfer coupling, the difference between the zero-zero electronic transition frequencies of two chromophores, and the duration of the

detection window. In addition to determining time-resolved anisotropies, we also follow the time evolution of the excitation probabilities on the two chromophores. Comparing the difference in site excitation probability as a function of time to the time-resolved anisotropy gives some indication of how the net population transfer affects the observed anisotropy signal.

In Section 5 we examine the effects of vibronic relaxation and dephasing resulting from the coupling of the intra-chromophore vibrations to a thermal bath. A simplified Redfield theory is used to include these effects. The bath is seen to have a significant influence on the time-resolved anisotropy, causing the anisotropy oscillations due to coherent vibrational and excitonic motion to diminish in amplitude. It is found, however, that coherent oscillations can survive the introduction of fairly rapid vibrational relaxation. Section 6 summarizes our conclusions.

## 2. MODEL SYSTEM

We start this Section by describing the model chromophore pair. Each chromophore has a ground and an excited electronic state and a single vibrational degree of freedom. The minima of the potential energy curves for the ground and excited electronic states are spatially displaced from each other in the vibrational coordinate. The Hamiltonian for chromophore 1 has the form

$$H_1 = |g1\rangle H_{g1} \langle g1| + |e1\rangle (H_{e1} + \varepsilon_1) \langle e1| . \quad (2)$$

where  $|g1\rangle$  and  $|e1\rangle$  denote the ground and excited electronic states,  $H_{g1}$  and  $H_{e1}$  denote the corresponding nuclear Hamiltonians, and  $\varepsilon_1$  is the zero-zero electronic transition frequency. [20] We take  $\hbar = 1$  throughout this paper and thereby express energy in angular frequency units. The Hamiltonian for chromophore 2 has a form analogous to Eq. (2).

The chromophore pair has four electronic states:  $|gg\rangle$  ( $\equiv |g1g2\rangle$ ),  $|eg\rangle$ ,  $|ge\rangle$ , and  $|ee\rangle$ . We omit the site index on the electronic state except when not doing so would create ambiguity.

In  $|gg\rangle$ , both chromophores are in their respective ground electronic states,  $|eg\rangle$  and  $|ge\rangle$  are the singly excited states with chromophore 1 and chromophore 2 excited, respectively, and  $|ee\rangle$  is the doubly excited state. The doubly excited state does not participate in the electronic excitation transfer and is omitted in what follows, but could come into play in pump-probe measurements, where it can be used as the final (measuring) state. [12]

The two singly excited states are coupled by an excitation transfer interaction, which in the dipole-dipole approximation would have the form [14]

$$V = \frac{1}{R^3} [\hat{\mu}_1 \cdot \hat{\mu}_2 - \frac{3}{R^2} (\hat{\mu}_1 \cdot \mathbf{R})(\hat{\mu}_2 \cdot \mathbf{R})] \cong U(|eg\rangle\langle ge| + h.c.), \quad (3)$$

where

$$\begin{aligned} \hat{\mu}_1 &= \mu_1 \mathbf{e}_1 (|e1\rangle\langle g1| + h.c.) , \\ \hat{\mu}_2 &= \mu_2 \mathbf{e}_2 (|e2\rangle\langle g2| + h.c.) , \end{aligned} \quad (4)$$

are the electronic dipole moment operators for chromophores 1 and 2, with  $\mu_1$  and  $\mu_2$  denoting the magnitudes of the electronic transition dipole moments and  $\mathbf{e}_1$  and  $\mathbf{e}_2$  denoting the unit vectors in the direction of the electronic transition dipole moments of chromophores 1 and 2, respectively. In the last expression of Eq. (3), only the terms that nearly conserve electronic energy have been retained, and  $U$  is given by

$$U = \frac{1}{R_0^3} \mu_1 \mu_2 [(\mathbf{e}_1 \cdot \mathbf{e}_2) - \frac{3}{R_0^2} (\mathbf{e}_1 \cdot \mathbf{R}_0)(\mathbf{e}_2 \cdot \mathbf{R}_0)]. \quad (5)$$

Combining Eqs. (2-5), the Hamiltonian for the chromophore pair can be written as

$$H_{cp} = |gg\rangle[H_{g1} + H_{g2}]\langle gg| + |eg\rangle[H_{e1} + H_{g2} + \varepsilon_1]\langle eg| + |ge\rangle[H_{g1} + H_{e2} + \varepsilon_2]\langle ge| + V. \quad (6)$$

The notation we shall use to label the vibrational states of the chromophore pair in the site representation refers to each mode's vibrational quantum number with a subscript designating the electronic state. For example,  $|ge\rangle|m_g n_e\rangle$  is the state with chromophore 2 excited,  $m$  quanta of vibration in the ground state of chromophore 1 and  $n$  quanta of vibration in the excited state of chromophore 2.

The interaction of the chromophore pair with the laser pulse is governed in the dipole approximation by

$$V_e(t) = -\hat{\boldsymbol{\mu}}_{cp} \cdot \mathbf{E}(t) , \quad (7)$$

where  $\hat{\boldsymbol{\mu}}_{cp} = \hat{\boldsymbol{\mu}}_1 + \hat{\boldsymbol{\mu}}_2$ ,  $\mathbf{E}(t)$  is the electric field of the laser pulse, and  $\hat{\boldsymbol{\mu}}_1$  and  $\hat{\boldsymbol{\mu}}_2$  are the electronic dipole moment operators given by Eq. (4). We assume  $\mathbf{E}(t)$  to be a Gaussian laser pulse of the form

$$\mathbf{E}(t) = E_0 \mathbf{e}_L \exp(-t^2/2\tau_L^2) \cos \Omega t , \quad (8)$$

with amplitude  $E_0$ , width  $\tau_L$ , related to the FWHM intensity by

$$\tau_L = \frac{FWHM}{2\sqrt{\ln 2}} , \quad (9)$$

center frequency  $\Omega$  and polarization  $\mathbf{e}_L$ .

The detector consists of a collection of two-level systems with a transition frequency distribution taken to be Gaussian. The Hamiltonian for the  $i^{th}$  two-level detector, which is meant to play a role analogous to that of a specific mode of the quantized radiation field, is given by

$$H_d^i = |a^i\rangle E_a^i \langle a^i| + |b^i\rangle E_b^i \langle b^i| , \quad (10)$$

where  $|a^i\rangle$  and  $|b^i\rangle$  are the ground and excited states of the  $i^{th}$  detector two-level system, respectively, and  $\varepsilon_d^i = E_b^i - E_a^i$  is the corresponding transition frequency. The electronic dipole operator for the  $i^{th}$  two-level system has the form

$$\hat{\boldsymbol{\mu}}_d^i = \mu_d \mathbf{e}_d (|a^i\rangle \langle b^i| + |b^i\rangle \langle a^i|) , \quad (11)$$

where  $\mu_d$  is the magnitude of the transition dipole moment and  $\mathbf{e}_d$  is the unit vector specifying the detector orientation. We omit the index  $i$  on  $\mu_d$  and  $\mathbf{e}_d$ , taking all detector two-level systems to have the same transition moment regardless of the transition frequency. The interaction Hamiltonian of the chromophore pair with the  $i^{th}$  detector two-level system is taken to be

$$V_d^i = -\eta \hat{\boldsymbol{\mu}}_{cp} \cdot \hat{\boldsymbol{\mu}}_d^i, \quad (12)$$

where  $\eta$  is a constant that will cancel out in the anisotropy. We can make the rotating wave approximation in the chromophore pair-detector interaction, which amounts to only keeping those terms that nearly conserve energy. In that approximation, Eq. (12) can be written as

$$\begin{aligned} V_d^i = & -\eta \mu_1 \mu_d (\mathbf{e}_1 \cdot \mathbf{e}_d) (|b^i\rangle|gg\rangle\langle eg|\langle a^i| + h.c.) \\ & -\eta \mu_2 \mu_d (\mathbf{e}_2 \cdot \mathbf{e}_d) (|b^i\rangle|gg\rangle\langle ge|\langle a^i| + h.c.). \end{aligned} \quad (13)$$

Time-dependent perturbation theory is used to determine the state of the system (chromophore pair + detector) following an interaction with a laser pulse and an interaction between the chromophore pair and the detector. Starting in an initial state  $|gg\rangle|m_g n_g\rangle|a^i\rangle$ , in which the chromophore pair and the detector two-level system are in their respective ground electronic states, the probability amplitude for finding the chromophore pair in the vibrational state  $|m'_g n'_g\rangle$  of the ground electronic state and the detector excited to  $|b^i\rangle$  is given in the interaction picture by

$$\begin{aligned} \langle b^i | \langle m'_g n'_g | \langle gg | \tilde{\Psi}(t) \rangle = & - \int_{-\infty}^t d\tau \int_{-\infty}^{\tau} d\tau' \\ & \times \langle b^i | \langle m'_g n'_g | \langle gg | \tilde{V}_d^i(\tau) \tilde{V}_e(\tau') | gg \rangle | m_g n_g \rangle | a^i \rangle, \end{aligned} \quad (14)$$

where  $\tilde{V}_e(\tau)$  and  $\tilde{V}_d^i(\tau)$  are the previously defined interaction Hamiltonians, given in Eq. (7) and Eq. (13), respectively, transformed to the interaction picture,

$$\tilde{V}_e(t) = e^{iH_0 t} V_e(t) e^{-iH_0 t}, \quad (15)$$

$$\tilde{V}_d^i(t) = e^{iH_0 t} V_d^i e^{-iH_0 t}, \quad (16)$$

and

$$|\tilde{\Psi}(t)\rangle = e^{iH_0 t} |\Psi(t)\rangle, \quad (17)$$

with

$$H_0 = H_{cp} + H_d^i. \quad (18)$$

Notice that the reverse ordering, in which  $\tilde{V}_d^i(\tau')$  acts before  $\tilde{V}_e(\tau)$  is excluded from Eq. (14) under the rotating wave approximation of Eq. (13). The probability of finding the chromophore pair in the electronic ground state level  $|m'_g n'_g\rangle$  and the detector in  $|b^i\rangle$  is then given by the absolute value squared of Eq. (14):

$$P^i(t) = |\langle b^i | \langle m'_g n'_g | \langle gg | \tilde{\Psi}(t) \rangle|^2. \quad (19)$$

In order to calculate  $P_{\parallel}^i(t)$  and  $P_{\perp}^i(t)$ , we set  $\mathbf{e}_d$  parallel and perpendicular, respectively, to  $\mathbf{e}_L$ , and average over all possible orientations of the chromophore pair in the laboratory frame. For given initial and final states of the chromophore pair, we must sum  $P^i(t)$  over the distribution of the detector frequencies. Taking that distribution to be Gaussian and converting the sum over detector frequencies to an integral, the total excited state population of the detector for given initial and final chromophore pair states becomes

$$P(t) = \int_{-\infty}^{\infty} d\varepsilon_d D(\varepsilon_d - \bar{\varepsilon}_d) P(t, \varepsilon_d), \quad (20)$$

where

$$D(\varepsilon_d - \bar{\varepsilon}_d) = \frac{1}{\Delta\sqrt{\pi}} \exp \left\{ -(\varepsilon_d - \bar{\varepsilon}_d)^2 / \Delta^2 \right\}, \quad (21)$$

where  $\bar{\varepsilon}_d$  is the center of the detector frequency distribution,  $\Delta$  is its width, and  $P^i(t)$  has been rewritten as a function of  $\varepsilon_d$ .

The total detector population change is obtained by summing over all final states of the chromophore pair and a thermal distribution of initial states. The time-resolved anisotropy is calculated according to Eq. (1), where the observed emission rate is obtained from the time-dependent population of the detector using the expression

$$S_{\parallel(\perp)}(t) = \frac{P_{\parallel(\perp)}(t + \frac{\Delta t}{2}) - P_{\parallel(\perp)}(t - \frac{\Delta t}{2})}{\Delta t}, \quad (22)$$

in which  $\Delta t$  is the response time of the detector. By calculating the average rate of change in detector excited state population, as in Eq. (22), we crudely incorporate the finite time resolution of detection. [21]

### 3. SIMPLE ANALYTIC MODEL

In Section 2 we developed a model Hamiltonian with which to calculate time-resolved anisotropy for a pair of chromophores having multiple vibrational levels and taking into account time and frequency resolution effects encountered in experimental measurements. Before proceeding to examine these effects, we shall first investigate the properties of a far simpler system, ignoring coherent vibrational motion by keeping only the lowest vibrational level in each of the the singly excited electronic states,  $|eg\rangle|0_e0_g\rangle$  and  $|ge\rangle|0_g0_e\rangle$ , and the three lowest vibrational levels of the ground electronic state,  $|gg\rangle|0_g0_g\rangle$ ,  $|gg\rangle|1_g0_g\rangle$ , and  $|gg\rangle|0_g1_g\rangle$ . In their recent work, Xie [22], Wynne and Hochstrasser [12], and Knox and Gülen [13] considered similar model systems, determining that if the initial state (prior to excitation) and final state (following spontaneous or stimulated emission) is  $|gg\rangle|0_g0_g\rangle$ , then the initial anisotropy can take on values greater than 0.4. The theoretical maximum value of 0.7 is exhibited by pairs of chromophores with perpendicular transition dipole moments of equal magnitude. Both Wynne and Hochstrasser [12] and Knox and Gülen [13] have included a phenomenological treatment of relaxation between the excited states of the system. We ignore relaxation in this section, but the analytical results for the time-resolved anisotropy of the simple model considered here will illustrate the dependence of the anisotropy on the final state(s) of the system.

The Hamiltonian of the simplified chromophore pair becomes

$$H_{cp} = |gg\rangle\langle gg|\{E_{gg}|0_g0_g\rangle\langle 0_g0_g| + (E_{gg} + \omega)|1_g0_g\rangle\langle 1_g0_g| + (E_{gg} + \omega)|0_g1_g\rangle\langle 0_g1_g|\} \\ + |eg\rangle\langle eg|E_{eg}|0_e0_g\rangle\langle 0_e0_g| + |ge\rangle\langle ge|E_{ge}|0_g0_e\rangle\langle 0_g0_e| + U(|eg\rangle\langle ge| |0_e0_g\rangle\langle 0_g0_e| + h.c.) , \quad (23)$$

Diagonalizing the excited state portion of  $H_{cp}$  yields the exciton states of the system, given by [23]

$$|+\rangle = \sin \frac{\theta}{2} |ge\rangle|0_g0_e\rangle + \cos \frac{\theta}{2} |eg\rangle|0_e0_g\rangle , \\ |-\rangle = \cos \frac{\theta}{2} |ge\rangle|0_g0_e\rangle - \sin \frac{\theta}{2} |eg\rangle|0_e0_g\rangle , \quad (24)$$

where  $\tan \theta$  is

$$\tan \theta = \frac{2U\langle 0_e 0_g | 0_g 0_e \rangle}{E_{eg} - E_{ge}}, \quad (25)$$

and the eigenenergies are

$$E_{\pm} = \frac{1}{2}(E_{eg} + E_{ge}) \pm \frac{1}{2}\sqrt{(E_{eg} - E_{ge})^2 + 4U^2\langle 0_e 0_g | 0_g 0_e \rangle^2}. \quad (26)$$

The form of the dipole moment operator in the exciton representation becomes

$$\begin{aligned} \hat{\boldsymbol{\mu}}_{cp} = & \boldsymbol{\mu}_+ \{|gg\rangle|0_g 0_g\rangle\langle +| + h.c.\} + \boldsymbol{\mu}_- \{|gg\rangle|0_g 0_g\rangle\langle -| + h.c.\} \\ & + \boldsymbol{\mu}_1 \langle 1_g 0_g | 0_e 0_g \rangle \{ \cos \frac{\theta}{2} |gg\rangle|1_g 0_g\rangle\langle +| - \sin \frac{\theta}{2} |gg\rangle|1_g 0_g\rangle\langle -| + h.c.\} \\ & + \boldsymbol{\mu}_2 \langle 0_g 1_g | 0_g 0_e \rangle \{ \sin \frac{\theta}{2} |gg\rangle|0_g 1_g\rangle\langle +| + \cos \frac{\theta}{2} |gg\rangle|0_g 1_g\rangle\langle -| + h.c.\}, \end{aligned} \quad (27)$$

with  $\boldsymbol{\mu}_+$  and  $\boldsymbol{\mu}_-$  given by

$$\begin{aligned} \boldsymbol{\mu}_+ &= \boldsymbol{\mu}_2 \langle 0_g 0_g | 0_g 0_e \rangle \sin \frac{\theta}{2} + \boldsymbol{\mu}_1 \langle 0_g 0_g | 0_e 0_g \rangle \cos \frac{\theta}{2}, \\ \boldsymbol{\mu}_- &= \boldsymbol{\mu}_2 \langle 0_g 0_g | 0_g 0_e \rangle \cos \frac{\theta}{2} - \boldsymbol{\mu}_1 \langle 0_g 0_g | 0_e 0_g \rangle \sin \frac{\theta}{2}. \end{aligned} \quad (28)$$

In addition to simplifying the chromophore pair model, we also simplify the interaction with the laser pulse and the detector by assuming that the excitation pulse duration and the detection window are both much shorter than the timescales of dynamics in the excited electronic state. Under these conditions, the rate of emission,  $S(t)$ , can be obtained by differentiating both sides of Eq. (20) with respect to time,

$$S(t) = \int_{-\infty}^{\infty} d\varepsilon_d D(\varepsilon_d - \bar{\varepsilon}_d) S(t, \varepsilon_d), \quad (29)$$

where  $S(t, \varepsilon_d)$  is the time derivative of  $P(t, \varepsilon_d)$  given by Eq. (19) and  $D(\varepsilon_d - \bar{\varepsilon}_d)$  is defined in Eq. (21). The probability amplitude for finding the system in  $|gg\rangle|0_g 0_g\rangle|b\rangle$ , starting in the initial state  $|gg\rangle|0_g 0_g\rangle|a\rangle$ , is given in the interaction picture by

$$\begin{aligned} \langle b | \langle 0_g 0_g | \langle gg | \tilde{\Psi}(t) \rangle = & -\frac{1}{\sqrt{2}} \sqrt{\pi} \tau_L E_0 \eta \mu_+^2 \mu_d (\mathbf{e}_+ \cdot \mathbf{e}_L) (\mathbf{e}_+ \cdot \mathbf{e}_d) \int_0^t d\tau \exp i(\varepsilon_d - \varepsilon_{+g}) \tau \\ & -\frac{1}{\sqrt{2}} \sqrt{\pi} \tau_L E_0 \eta \mu_-^2 \mu_d (\mathbf{e}_- \cdot \mathbf{e}_L) (\mathbf{e}_- \cdot \mathbf{e}_d) \int_0^t d\tau \exp i(\varepsilon_d - \varepsilon_{-g}) \tau, \end{aligned} \quad (30)$$

where  $\varepsilon_{\pm g} = E_{\pm} - E_{gg}$  and  $\boldsymbol{\mu}_{\pm} \equiv \mu_{\pm} \mathbf{e}_{\pm}$ . Calculating  $S(t, \varepsilon_d)$ , integrating over the frequency profile of the detector according to Eq. (29), and taking  $\Delta \gg |\varepsilon_{+-}|$  where  $\varepsilon_{+-} = E_+ - E_-$  yields

$$S(t) = \frac{1}{2}\pi\tau_L^2 E_0^2 \eta^2 \mu_+^4 \mu_d^2 (\mathbf{e}_+ \cdot \mathbf{e}_L)^2 (\mathbf{e}_+ \cdot \mathbf{e}_d)^2 + \frac{1}{2}\pi\tau_L^2 E_0^2 \eta^2 \mu_-^4 \mu_d^2 (\mathbf{e}_- \cdot \mathbf{e}_L)^2 (\mathbf{e}_- \cdot \mathbf{e}_d)^2 + \pi\tau_L^2 E_0^2 \eta^2 \mu_+^2 \mu_-^2 \mu_d^2 (\mathbf{e}_+ \cdot \mathbf{e}_L) (\mathbf{e}_+ \cdot \mathbf{e}_d) (\mathbf{e}_- \cdot \mathbf{e}_L) (\mathbf{e}_- \cdot \mathbf{e}_d) \cos(\varepsilon_{+-} t). \quad (31)$$

The first two terms in Eq. (31) result from excitation and emission via  $|+\rangle$  and  $|-\rangle$ , respectively, and the third (oscillatory) term results from interference in emission from  $|+\rangle$  and  $|-\rangle$ . While the internal geometry of the chromophore pair is assumed to be fixed, it can be randomly oriented in space. To average Eq. (31) over spatial orientations, we integrate  $\mathbf{e}_+$  over  $4\pi$  of solid angle and, maintaining a fixed angle between  $\mathbf{e}_+$  and  $\mathbf{e}_-$ , integrate the latter over  $2\pi$  radians. Defining a direction cosine

$$\cos \gamma = \mathbf{e}_+ \cdot \mathbf{e}_-, \quad (32)$$

the orientationally averaged signal is given by (see Appendix)

$$S_{\parallel}^{avg}(t) = \frac{\pi\tau_L^2 E_0^2 \eta^2 \mu_d^2}{2} \left\{ \frac{1}{5}(\mu_+^4 + \mu_-^4) + 2\mu_+^2 \mu_-^2 \left( \frac{1}{5} \cos^2 \gamma + \frac{1}{15} \sin^2 \gamma \right) \cos(\varepsilon_{+-} t) \right\}, \quad (33)$$

$$S_{\perp}^{avg}(t) = \frac{\pi\tau_L^2 E_0^2 \eta^2 \mu_d^2}{2} \left\{ \frac{1}{15}(\mu_+^4 + \mu_-^4) + 2\mu_+^2 \mu_-^2 \left( \frac{1}{15} \cos^2 \gamma - \frac{1}{30} \sin^2 \gamma \right) \cos(\varepsilon_{+-} t) \right\}. \quad (34)$$

Using Eqs. (33) and (34) in Eq. (1) gives the time-dependent anisotropy

$$R(t) = \frac{2(\mu_+^4 + \mu_-^4) + \mu_+^2 \mu_-^2 (4 + \cos^2 \gamma) \cos(\varepsilon_{+-} t)}{5(\mu_+^4 + \mu_-^4) + 10\mu_+^2 \mu_-^2 \cos^2 \gamma \cos(\varepsilon_{+-} t)}. \quad (35)$$

Let us now examine the case of identical chromophores. In that case, and assuming  $\theta = \frac{\pi}{2}$  in Eq. (25), the expressions for  $\mu_+$  and  $\mu_-$  in Eq. (28) simplify to

$$\mu_{\pm} \mathbf{e}_{\pm} = \frac{1}{\sqrt{2}} \langle 0_g 0_g | 0_e 0_g \rangle (\mu_2 \mathbf{e}_2 \pm \mu_1 \mathbf{e}_1). \quad (36)$$

Because  $\mu_1 = \mu_2$ , the two transition dipole moments in Eq. (36) are perpendicular. Substituting  $\gamma = \frac{\pi}{2}$  into Eq. (35) yields

$$R(t) = \frac{2(\mu_+^4 + \mu_-^4) + 3\mu_+^2\mu_-^2 \cos(\varepsilon_{+-}t)}{5(\mu_+^4 + \mu_-^4)} . \quad (37)$$

The expression (37) for the time-resolved anisotropy can be restated in terms of the angle between the directions of the transition dipole moments of the two chromophores,  $\mathbf{e}_1$  and  $\mathbf{e}_2$ . Calling that angle  $\phi$ , Eq. (37) becomes (see Appendix)

$$R(t) = 0.4 + 0.3 \frac{1 - \cos^2 \phi}{1 + \cos^2 \phi} \cos(\varepsilon_{+-}t) . \quad (38)$$

The denominator of Eq. (37) is proportional to the total intensity and is time-independent. The time-independent overall intensity results from the fact that the chromophore pairs are identical and randomly distributed. When transitions to both exciton states are optically bright, the oscillatory term initially enhances the parallel signal while diminishing the perpendicular signal, resulting in an initial anisotropy larger than 0.4. Alternatively, if one of the exciton states is optically dark, the interference term vanishes and the anisotropy is 0.4 and time-independent. The maximum anisotropy can be attained when the interference term is maximized, which occurs when  $\mathbf{e}_1$  and  $\mathbf{e}_2$  are perpendicular.

Let us now compare the anisotropy in Eq. (38) with the anisotropy that would be obtained if the only admitted final states of the chromophore pair were  $|gg\rangle|1_g0_g\rangle$  and  $|gg\rangle|0_g1_g\rangle$ , the two electronic ground states with one of the chromophores in the first vibrationally excited state. The probability amplitude of finding the system in  $|gg\rangle|1_g0_g\rangle|b\rangle$ , starting in the initial state  $|gg\rangle|0_g0_g\rangle|a\rangle$  with an excitation pulse short on the timescale of excited state dynamics, is

$$\begin{aligned} \langle b | \langle 1_g0_g | \langle gg | \tilde{\Psi}(t) \rangle = & -\frac{1}{\sqrt{2}} \sqrt{\pi} \tau_L E_0 \eta \mu_d \cos \frac{\theta}{2} \langle 0_e0_g | 1_g0_g \rangle \mu_+ \mu_1 (\mathbf{e}_+ \cdot \mathbf{e}_L) (\mathbf{e}_1 \cdot \mathbf{e}_d) \\ & \times \int_0^t d\tau \exp i(\varepsilon_d - \varepsilon_{+g} + \omega)\tau \\ & + \frac{1}{\sqrt{2}} \sqrt{\pi} \tau_L E_0 \eta \mu_d \sin \frac{\theta}{2} \langle 0_e0_g | 1_g0_g \rangle \mu_- \mu_1 (\mathbf{e}_- \cdot \mathbf{e}_L) (\mathbf{e}_1 \cdot \mathbf{e}_d) \\ & \times \int_0^t d\tau \exp i(\varepsilon_d - \varepsilon_{-g} + \omega)\tau . \end{aligned} \quad (39)$$

Since the Franck-Condon factor between states  $|0_g0_e\rangle$  and  $|1_g0_g\rangle$  vanishes, there is no  $\mathbf{e}_2$  component present in emission from  $|+\rangle$  and  $|-\rangle$  into  $|gg\rangle|1_g0_g\rangle$ . The rate of emission,

obtained in the same manner as Eq. (31), is

$$\begin{aligned}
S(t) = & \frac{1}{2}\pi\tau_L^2 E_0^2 \eta^2 \mu_+^2 \mu_1^2 \mu_d^2 \cos^2 \frac{\theta}{2} \langle 0_e 0_g | 1_g 0_g \rangle^2 \overline{(\mathbf{e}_+ \cdot \mathbf{e}_L)^2 (\mathbf{e}_1 \cdot \mathbf{e}_d)^2} \\
& + \frac{1}{2}\pi\tau_L^2 E_0^2 \eta^2 \mu_-^2 \mu_1^2 \mu_d^2 \sin^2 \frac{\theta}{2} \langle 0_e 0_g | 1_g 0_g \rangle^2 \overline{(\mathbf{e}_- \cdot \mathbf{e}_L)^2 (\mathbf{e}_1 \cdot \mathbf{e}_d)^2} \\
& + \pi\tau_L^2 E_0^2 \eta^2 \mu_+ \mu_- \mu_1^2 \mu_d^2 \sin \frac{\theta}{2} \cos \frac{\theta}{2} \langle 0_e 0_g | 1_g 0_g \rangle^2 \overline{(\mathbf{e}_+ \cdot \mathbf{e}_L)(\mathbf{e}_- \cdot \mathbf{e}_L)(\mathbf{e}_1 \cdot \mathbf{e}_d)^2} \cos(\varepsilon_{+-} t) , \quad (40)
\end{aligned}$$

where the overbar signifies orientational averaging. The rate of emission into  $|gg\rangle|0_g 1_g\rangle$  has an identical form to Eq. (40). The time-resolved anisotropy for the case of identical chromophores now takes the form

$$R(t) = \frac{2(\mu_+^4 + \mu_-^4) + \mu_+^2 \mu_-^2 (6 \cos(\varepsilon_{+-} t) - 2)}{5(\mu_+^2 + \mu_-^2)^2} \quad (41)$$

in terms of the transition moments of the exciton states or, alternatively,

$$R(t) = 0.1 + 0.3 \cos^2 \phi + 0.3(1 - \cos^2 \phi) \cos(\varepsilon_{+-} t) , \quad (42)$$

where  $\phi$  is the angle between  $\mathbf{e}_1$  and  $\mathbf{e}_2$ . The time zero anisotropy predicted by Equations (41) and (42) is 0.4, independent of the angle between  $\mathbf{e}_1$  and  $\mathbf{e}_2$ .

The qualitative difference between anisotropies described by Eqs. (38) and (42) at  $t = 0$  can be understood by considering Eqs. (31) and (40) in the short time limit where  $\cos(\varepsilon_{+-} \delta t) \cong 1$ . The emission rate in Eq. (31) at  $\delta t$  becomes

$$\begin{aligned}
S(\delta t) \cong & \frac{1}{2}\pi\tau_L^2 E_0^2 \eta^2 \mu_1^4 \mu_d^2 \langle 0_g 0_g | 0_e 0_g \rangle^2 \overline{(\mathbf{e}_1 \cdot \mathbf{e}_L)^2 (\mathbf{e}_1 \cdot \mathbf{e}_d)^2} \\
& + \frac{1}{2}\pi\tau_L^2 E_0^2 \eta^2 \mu_2^4 \mu_d^2 \langle 0_g 0_g | 0_g 0_e \rangle^2 \overline{(\mathbf{e}_2 \cdot \mathbf{e}_L)^2 (\mathbf{e}_2 \cdot \mathbf{e}_d)^2} \\
& + \pi\tau_L^2 E_0^2 \eta^2 \mu_1^2 \mu_2^2 \mu_d^2 \langle 0_g 0_g | 0_e 0_g \rangle \langle 0_g 0_g | 0_g 0_e \rangle \overline{(\mathbf{e}_1 \cdot \mathbf{e}_L)(\mathbf{e}_2 \cdot \mathbf{e}_L)(\mathbf{e}_1 \cdot \mathbf{e}_d)(\mathbf{e}_2 \cdot \mathbf{e}_d)} , \quad (43)
\end{aligned}$$

where we have used Eq. (28) to express the rate in terms of the site transition dipole moments. Carrying out the orientational average (see Eq. (88) of the Appendix) and calculating the the anisotropy yields

$$R(\delta t) = \frac{2\mu_1^4 \langle 0_g 0_g | 0_e 0_g \rangle^2 + 2\mu_2^4 \langle 0_g 0_g | 0_g 0_e \rangle^2 + \mu_1^2 \mu_2^2 (\cos^2 \phi + 3) \langle 0_g 0_g | 0_e 0_g \rangle \langle 0_g 0_g | 0_g 0_e \rangle}{5\mu_1^4 \langle 0_g 0_g | 0_e 0_g \rangle^2 + 5\mu_2^4 \langle 0_g 0_g | 0_g 0_e \rangle^2 + 10\mu_1^2 \mu_2^2 \cos^2 \phi \langle 0_g 0_g | 0_e 0_g \rangle \langle 0_g 0_g | 0_g 0_e \rangle} , \quad (44)$$

where  $\phi$  is the angle between  $\mathbf{e}_1$  and  $\mathbf{e}_2$ . The first two terms in the numerator and the denominator of Eq. (44) arise from contributions involving each chromophore separately, while the third term results from contributions from both chromophores. This crossterm depends on the angle between the dipole moments of the chromophores, and the short-time anisotropy has its maximum when  $\phi = \frac{\pi}{2}$ . On the other hand, the rate of emission into  $|gg\rangle|1_g0_g\rangle$ , given in Eq. (40), becomes

$$S(\delta t) \cong \frac{1}{2}\pi\tau_L^2 E_0^2 \eta^2 \mu_1^4 \mu_d^2 \langle 0_g0_g|0_e0_g \rangle \langle 0_e0_g|1_g0_g \rangle \overline{(\mathbf{e}_1 \cdot \mathbf{e}_L)^2 (\mathbf{e}_1 \cdot \mathbf{e}_d)^2}, \quad (45)$$

where Eq. (28) was again used to express the rate in terms of transition dipole moments of the individual monomers. Carrying out the orientational average and calculating the anisotropy yields  $R(\delta t) = 0.4$ . There is no crossterm in Eq. (45) analogous to the one in Eq. (43) because transitions from  $|eg\rangle|0_e0_g\rangle$  to  $|gg\rangle|0_g1_g\rangle$  and from  $|ge\rangle|0_g0_e\rangle$  to  $|gg\rangle|1_g0_g\rangle$  are Franck-Condon forbidden. There is only one route to each final state in this case, and quantum mechanical interference in emission from the two sites does not occur. Therefore, the  $t = 0$  anisotropy given by Eq. (38) is sensitive to the presence of both chromophores, while the anisotropy given in Eq. (42) is not. It is worth emphasizing that the high initial value of the anisotropy predicted by Eq. (44) reflects the fixed relative geometry of the chromophore pair, rather than the presence of energy transfer, *per se*. The lack of dependence of  $S(\delta t)$  in Eqs. (43) and (45) on the exciton splitting is in keeping with that fact.

Although it might appear in Eq. (38) as though  $R(t)$  would exhibit oscillations whenever  $\phi \neq 0$ , this is not always the case. For example, in the case when  $\phi = \frac{\pi}{2}$  and either  $\mathbf{e}_1$  or  $\mathbf{e}_2$  lies along the inter-chromophore axis, the energy splitting between the exciton states will be zero, assuming dipolar coupling of the form given in Eq. (3), and the anisotropy will be time-independent. Conversely, excitation transfer is not always required for the anisotropy to exhibit oscillations. The anisotropy given by Eq. (35), which applies to chromophores that are not necessarily identical, will exhibit oscillations even in the case of zero excitation transfer coupling, as long as the individual chromophores have different electronic transition frequencies.

From the calculation presented in this Section we see that time-resolved anisotropy in a multilevel system will contain both kinds of contributions described by Eqs. (38) and (42), and that proper treatment of time-resolved fluorescence anisotropy must include the multilevel structure of both the excited and ground electronic states of the chromophores. The relative weights of the contributions leading to the anisotropies given in Eqs. (38) and (42) will be determined by the spectral characteristics of the excitation and detection processes. Generally speaking, contributions giving rise to the standard (0.4) value of the initial anisotropy are expected to outweigh the contributions of the kind described by Eq. (38), especially when higher vibrational states of the ground electronic state are selected as the final states by the detection process, which is often the case with fluorescence upconversion.

[4]

#### 4. EFFECTS OF VIBRATIONAL MOTION AND EXCITATION/DETECTION CONDITIONS

The analysis of Section 3, despite using a simplified model chromophore pair and neglecting effects of less-than-ideal excitation and detection conditions, serves to demonstrate the importance of properly including the vibrational structure of initial and final states when calculating the fluorescence anisotropy. In this Section, we will utilize the model developed in Section 2 more fully, including the full vibrational level structure of both chromophores and non-zero duration for the excitation pulse and the detection window.

The model in Section 2 was developed in the site representation in order to give a better physical picture of different features of the model. The calculations in this Section, like those in Section 3, are more conveniently carried out in the energy eigenstate representation. The chromophore pair Hamiltonian in the eigenstate representation can be written as

$$H_{cp} = \sum_{\alpha} |\alpha\rangle E_{\alpha} \langle \alpha| + \sum_{\gamma} |\gamma\rangle E_{\gamma} \langle \gamma| \quad (46)$$

where, for simplicity of notation, we denote all eigenstates in the ground electronic manifold

of the chromophore pair by  $\alpha$  and all exciton states by  $\gamma$ , with  $E_\alpha$  and  $E_\gamma$  as the corresponding angular frequencies. The electronic dipole operator can be expressed as

$$\hat{\mathbf{\mu}}_{cp} = \sum_{\alpha,\gamma} \mu_{\alpha\gamma} \mathbf{e}_{\alpha\gamma} (|\alpha\rangle\langle\gamma| + |\gamma\rangle\langle\alpha|) , \quad (47)$$

where  $\mu_{\alpha\gamma} \mathbf{e}_{\alpha\gamma}$  is the transition dipole moment between states  $|\alpha\rangle$  and  $|\gamma\rangle$ .

Starting in the initial state  $|\alpha\rangle|a\rangle$ , the probability amplitude for finding the system in a final state  $|\alpha'\rangle|b\rangle$  following an interaction with a laser pulse and the detector is given by (see Eq. (14))

$$\langle b|\langle\alpha'|\tilde{\Psi}(t)\rangle = -\frac{E_0\eta\mu_d}{2} \sum_{\gamma} \mu_{\alpha\gamma} \mu_{\alpha'\gamma} (\mathbf{e}_{\alpha\gamma} \cdot \mathbf{e}_L) (\mathbf{e}_{\alpha'\gamma} \cdot \mathbf{e}_d) \int_{-\infty}^t d\tau \int_{-\infty}^{\tau} d\tau_1 \times \exp\{i(\varepsilon_d - \varepsilon_{\gamma\alpha'})\tau\} \exp\{i(\varepsilon_{\gamma\alpha} - \Omega)\tau_1\} \exp\{-\tau_1^2/2\tau_L^2\} . \quad (48)$$

Calculating the excited state population in  $|b\rangle$  according to Eq. (19) and integrating over the frequency profile of the detector according to Eq. (20) yields

$$\begin{aligned} P(t, \bar{\varepsilon}_d) = & \frac{E_0^2 \eta^2 \mu_d^2}{4} \sum_{\gamma, \gamma'} \mu_{\alpha\gamma} \mu_{\alpha\gamma'} \mu_{\alpha'\gamma} \mu_{\alpha'\gamma'} (\mathbf{e}_{\alpha\gamma} \cdot \mathbf{e}_L) (\mathbf{e}_{\alpha\gamma'} \cdot \mathbf{e}_L) (\mathbf{e}_{\alpha'\gamma} \cdot \mathbf{e}_d) (\mathbf{e}_{\alpha'\gamma'} \cdot \mathbf{e}_d) \\ & \times \int_{-\infty}^t d\tau \int_{-\infty}^{\tau} d\tau_1 \int_{-\infty}^t d\tau_2 \int_{-\infty}^{\tau_2} d\tau_3 \exp\{-(\tau - \tau_2)^2 \Delta^2/4\} \\ & \times \exp\{-i(\bar{\varepsilon}_d - \varepsilon_{\gamma'\alpha'})\tau\} \exp\{-i(\varepsilon_{\gamma'\alpha} - \Omega)\tau_1\} \exp\{-\tau_1^2/2\tau_L^2\} \\ & \times \exp\{i(\bar{\varepsilon}_d - \varepsilon_{\gamma\alpha'})\tau_2\} \exp\{i(\varepsilon_{\gamma\alpha} - \Omega)\tau_3\} \exp\{-\tau_3^2/2\tau_L^2\} \end{aligned} \quad (49)$$

As discussed in Section 2, the total excited state population is calculated by summing Eq. (49) over all final states and thermally weighted initial states of the chromophore pair.

The average, over chromophore pair orientations, of the products of four direction cosines appearing in Eq. (49) must now be carried out. It is convenient to express the transition moments  $\mathbf{e}_{\alpha\gamma} \mu_{\alpha\gamma}$  in terms of  $\mathbf{e}_1 \mu_1$  and  $\mathbf{e}_2 \mu_2$ , the transition dipole moments of the individual chromophores,

$$\mathbf{e}_{\alpha\gamma} \mu_{\alpha\gamma} = \langle \alpha | gg \rangle \langle eg | \gamma \rangle \mathbf{e}_1 \mu_1 + \langle \alpha | gg \rangle \langle ge | \gamma \rangle \mathbf{e}_2 \mu_2 . \quad (50)$$

Using Eq. (50) enables us to express the product of four direction cosines in Eq. (49) in terms of direction cosines involving  $\mathbf{e}_1$  and  $\mathbf{e}_2$ . There are four different orientational

averages to perform. These averages are given in the Appendix. Eq. (49) can now be used to compute the population in the excited state of the detector, and subsequently the time-resolved fluorescence anisotropy using Eq. (22).

In the numerical calculation presented in this Section, we have chosen the parameters for the chromophore pair to roughly correspond to the known parameters in the closely-coupled chromophore pairs consisting of  $\alpha$ -84 and  $\beta$ -84 tetrapyrroles on adjacent monomers in C-PC trimers. [4] The value of the excitation transfer coupling matrix element is set to  $-50 \text{ cm}^{-1}$  ( $1 \text{ cm}^{-1}$  corresponds to an angular frequency of  $1.885 \times 10^{11} \text{ s}^{-1}$ ), corresponding to Sauer and Scheer's calculation of the excitonic interaction energy. [24] The angle between the transition moments of the chromophores is set to  $65^\circ$ , corresponding to the value estimated from the x-ray crystallographic structure. [5] The zero-zero electronic transition frequency of chromophore 2 is taken to be  $150 \text{ cm}^{-1}$  higher than that of chromophore 1. This offset corresponds to the difference in absorption maxima of the  $\alpha$ -84 and  $\beta$ -84 chromophores. [24,25] The potential energy curves for  $H_{g1}$ ,  $H_{g2}$ ,  $H_{e1}$ , and  $H_{e2}$  are chosen to be harmonic and to have the same frequency of  $100 \text{ cm}^{-1}$ . This choice of vibrational frequency is arbitrary, but is typical of a low frequency molecular vibration and is in the interesting range comparable to the frequencies of pure exciton dynamics. In the absence of experimental data, we assume a small displacement between ground and excited potential energy curves on each chromophore of 1.5 times the rms width of the ground state coordinate distribution,  $\frac{1}{\sqrt{2\omega}}$  for a mass-weighted oscillator coordinate. The excitation laser pulse is taken to be 70 fs Full Width at Half Maximum (FWHM) in intensity ( $\tau_L = 42 \text{ fs}$ ), in accordance with experiment. [4] The frequency resolution of the detector is set to  $210 \text{ cm}^{-1}$  FWHM in intensity ( $\Delta = 126 \text{ cm}^{-1}$ ), which corresponds to the frequency width of the detection window used in the experiments, [4] and the width of the time detection window is taken to be 70 fs. The radiative lifetimes of the excited states are much longer than our timescale of interest of a few picoseconds, and non-radiative excited state population decay mechanisms, such as intersystem crossing, are ignored. The initial state of the chromophore pair is  $|gg\rangle|0,0_g\rangle$  for all calculations in this section. See Section 5 for calculations that include additional thermally populated initial

states.

Figure 1 shows time-dependent anisotropies calculated for the model system using the parameters listed above. Two different sets of excitation and detection conditions are illustrated. The upper (thick) curve in Figure 1 was calculated with  $\Omega$ , the center frequency of the laser pulse, resonant with  $\varepsilon_1$ , the zero-zero electronic transition frequency of chromophore 1. The lower (thin) curve was calculated with  $\Omega$  at  $100\text{ cm}^{-1}$  above  $\varepsilon_2$ , the zero-zero electronic transition frequency of the chromophore 2. In each case, the average detector frequency,  $\bar{\varepsilon}_d$ , was centered  $250\text{ cm}^{-1}$  below  $\Omega$ . We included 30 states in the singly excited manifold, allowing up to 4 quanta of combined vibrational excitation, and 28 states in the ground manifold, allowing up to 6 quanta of combined vibrational excitation. Inclusion of additional states in the ground or the excited manifold had no effect on the calculated anisotropy.

The difference in excitation and detection conditions in the two cases gives rise to qualitative differences in the anisotropy. Anisotropies in Figure 1 exhibit complicated behavior that contains effects of both exciton dynamics (including excitation transfer) and nuclear dynamics. It can be seen from the near constancy of the anisotropy that little change occurs in the emission polarization direction when the excitation pulse only weakly populates the excited states of the higher-energy chromophore (thick curve). The absence of exciton dynamics is reflected in the weak time-dependence and relatively high value of the anisotropy. On the other hand, anisotropy resulting from excitation at  $100\text{ cm}^{-1}$  above the zero-zero electronic transition frequency of the higher-energy chromophore, shown by the lower (thin) curve in Figure 1, resonantly populates a range of states having amplitude on both chromophores, leading to a larger extent of excitation transfer, as evidenced by the large oscillations in the anisotropy. The dependence of the anisotropy on the excitation frequency in our calculations shows a similar trend to the experimental results of Xie *et al.* [4], who found that excitation at the red edge of the absorption spectrum of the chromophore pairs in APC and C-PC trimers resulted in a more weakly time-dependent anisotropy with higher asymptotic values than excitation at a higher frequency.

One feature common to the two plots in Figure 1 is their high initial anisotropy and

subsequent rapid decrease during the first 0.1 ps. Despite the difference in site energy between the chromophores and the finite bandwidth of the excitation pulse and the detector, both chromophores can be excited at short times and the interference in emission necessary for anisotropy greater than 0.4 can occur. When the excitation pulse and the detection window overlap, both are effectively shortened by the requirement that the former must act before the latter. In addition, the nuclear wave packets  $|\psi_{eg}(t)\rangle$  and  $|\psi_{ge}(t)\rangle$  prepared in the Franck-Condon regions of the two excited state potential energy surfaces both resemble  $|0_g 0_g\rangle$  at short times, favoring emission into the same ground state. Thus, the initial anisotropy is dominated by terms of the kind illustrated by Eq. (38).

The effective frequency resolution improves once the pulses cease to overlap and each can operate for its full duration. Moreover, since  $|\psi_{eg}(t)\rangle$  and  $|\psi_{ge}(t)\rangle$  move differently on their respective potential energy surfaces, nuclear motion favors emission to non-overlapping final states, decreasing the effect of quantum mechanical interference in the anisotropy. It should also be mentioned that the site energy difference between the two chromophores contributes to a differing rate of phase accumulation, which leads to an overall sinusoidal oscillation in the anisotropy. All of these factors can contribute to a rapid decrease in the anisotropy, even in the absence of energy transfer coupling between the sites. For this reason, the rapid “decay” of the anisotropies of Figure 1 cannot automatically be regarded as a manifestation of ultrafast energy transfer.

In the calculations presented in Figure 1, the time detection window  $\Delta t$  was taken to be 70 fs, equal to the FWHM duration of the excitation pulse and the time corresponding to the FWHM frequency width of the detector. However, experimental time resolution can often be lower than the inverse frequency width of the detector. Figure 2 compares the anisotropy shown in the lower (thin) curve of Figure 1 with the anisotropy calculated using identical parameters except that the time detection window,  $\Delta t$ , was lengthened to 150 fs. The  $t = 0$  anisotropy drops considerably as the time resolution decreases. Therefore, limitations in the experimental time resolution can prevent observation of the high initial anisotropy discussed above.

Figure 3 shows time-dependent anisotropies calculated with the same parameters as those used in Figure 1 except that the offset between the zero-zero electronic transition frequencies of the two chromophores is decreased to  $100 \text{ cm}^{-1}$  (i.e. equal to the vibrational level spacing) by decreasing the zero-zero transition frequency  $\varepsilon_2$  of the higher-energy chromophore, resulting in more efficient excitation transfer because many vibronic levels of the two chromophores are now in resonance. Because the excitation frequencies were kept the same as those in Figure 1, the  $\Omega$  value for the lower (thin) curve in Figure 3 is now  $150 \text{ cm}^{-1}$  above the zero-zero electronic transition frequency of the higher-energy chromophore. The time-resolved anisotropies in Figure 3 show considerable differences from those of Figure 1. The lower (thin) curve in Figure 3 exhibits more frequent large oscillations, due to more efficient energy transfer between the singly excited states. The upper (thick) curve in Figure 3 shows an increase, relative to the corresponding case of Figure 1, in the magnitude of oscillation, consistent with the fact that there is now more spectral overlap of the excitation pulse with states having significant amplitude on the higher-energy as well as the lower-energy chromophore.

In Figure 4, time-resolved anisotropies are shown for a case of two identical chromophores, with the same excitation and detection conditions as in the previous calculations. The anisotropies can be seen to reflect the fact that this is the case with the most efficient excitation transfer. The frequency of the large amplitude oscillations is the highest compared to Figures 1 and 3 in the case of excitation  $250 \text{ cm}^{-1}$  above the zero-zero electronic transition frequency of the chromophores (thin curve). Excitation at the zero-zero electronic transition frequency of the chromophores (thick curve) shows the largest extent of excitation transfer (even leading to a negative anisotropy at  $t \approx 330 \text{ fs}$ ) compared to its counterparts in Figures 1 and 3.

Figure 5 examines the dependence of the initial ( $t = 0$ ) anisotropy on the strength of the excitation transfer coupling while the rest of the parameters are kept constant. As the excitation transfer coupling is increased, the initial anisotropy decreases because the initial rapid decrease of the anisotropy, calculated before time averaging according to Eq. (22)

(not shown), becomes more rapid with increasing coupling, and keeping the time-resolution of the detector constant results in observing a lower average anisotropy during the  $t = 0$  detection window. It is evident that for the case where the timescale of exciton dynamics is shorter than the timescale of the excitation and detection process, the high initial anisotropy will not be observed.

The time-resolved anisotropy reflects the exciton dynamics of the chromophore pair. It would be interesting to determine the extent to which the time-resolved anisotropy manifests the net transfer of excited state population between the chromophores. [3] The time-dependent site population difference is given by  $\langle \Psi(t) | P_1 - P_2 | \Psi(t) \rangle$ , where  $|\Psi(t)\rangle$  is the state of the chromophore pair at time  $t$ , and  $P_1$  and  $P_2$  are given by

$$P_1 = \sum_{n_e, m_g} |eg\rangle\langle eg| |n_e m_g\rangle\langle n_e m_g| \quad (51)$$

and

$$P_2 = \sum_{n_g, m_e} |ge\rangle\langle ge| |n_g m_e\rangle\langle n_g m_e| . \quad (52)$$

At times after the excitation pulse has subsided, the time-dependent orientationally averaged population difference can be expressed by

$$\begin{aligned} \langle \Psi(t) | P_1 - P_2 | \Psi(t) \rangle &= \sum_{\gamma, \gamma'} \mu_{\alpha\gamma} \mu_{\alpha\gamma'} \overline{(\mathbf{e}_{\alpha\gamma} \cdot \mathbf{e}_L) (\mathbf{e}_{\alpha\gamma'} \cdot \mathbf{e}_L)} \\ &\times F(\varepsilon_{\gamma\alpha} - \Omega) F(\varepsilon_{\gamma'\alpha} - \Omega) e^{iE_{\gamma, \gamma'} t} \langle \gamma | (P_1 - P_2) | \gamma' \rangle , \end{aligned} \quad (53)$$

where

$$F(\omega) = \sqrt{2\pi} \tau_L \exp(-\tau_L^2 \omega^2/2) . \quad (54)$$

Figure 6 shows the calculation of the expectation value of  $P_1(t) - P_2(t)$ , normalized by the total excited state population,  $P_1(t) + P_2(t)$ , for the same parameters as in Figure 1. Again, the initial state of the chromophore pair is taken to be  $|\alpha\rangle = |gg\rangle|0_g 0_g\rangle$ . The thick curve shown in Figure 6a is the time-dependent site population difference in the case of excitation centered at the zero-zero electronic transition frequency of chromophore 1, the lower-energy

chromophore, and the thin curve is the corresponding time-dependent anisotropy. In Figure 6b, the thick curve is the time-dependent site population difference for the excitation frequency centered  $100 \text{ cm}^{-1}$  above the zero-zero electronic transition frequency of (the higher-energy) chromophore 2, and the thin curve is the again the corresponding time-resolved anisotropy. The excitation condition that leads to the site population difference curve in Figure 6a places most of the initial excitation on chromophore 1, as evidenced by the positive initial value of  $\frac{P_1(t) - P_2(t)}{P_1(t) + P_2(t)}$ . The relatively small oscillations of the upper (thick) curve indicate that most of the excitation remains on the lower-energy chromophore. This is consistent with the anisotropy results shown in the thin curve of Figure 6a, where the time-resolved anisotropy obtained with the same excitation conditions shows relatively small oscillations and high anisotropy. Excitation centered  $100 \text{ cm}^{-1}$  above the zero-zero electronic transition frequency of the higher-energy chromophore, resulting in a site population difference shown in the thick curve of Figure 6b, also exhibits behavior consistent with the excitation conditions.  $\frac{P_1(t) - P_2(t)}{P_1(t) + P_2(t)}$  is initially negative, indicating that the excitation conditions place most of the excitation on the higher-energy chromophore; even though there is good spectral overlap between the excitation pulse and states on both chromophores, the Franck-Condon factors are more favorable for the excitation of the higher-energy chromophore for the coordinate displacement between ground and excited states that we have chosen. The large oscillations about a relatively low value of the site population difference indicate efficient net population transfer between the two chromophores. This behavior is also reflected in the large oscillations seen in the corresponding time-dependent anisotropy shown in the thin curve in Figure 6b. In fact, the first several extrema in the population difference of Figure 6b coincide with corresponding extrema in the anisotropy. In both Figs. 6a and 6b, however, the anisotropies show high frequency structure attributable to coherent vibrational motion, that is not as clearly evident in the excitation probability difference.

## 5. EFFECTS OF VIBRATIONAL RELAXATION AND DEPHASING

In the previous sections we developed a model for an isolated chromophore pair and a detector in order to describe the time-resolved fluorescence anisotropy following excitation with an ultrashort laser pulse. The time-resolved anisotropies shown in Section 4 exhibited a similarity in excitation wavelength dependence to the experimental measurements made on APC and C-PC. [4] The experimental anisotropy measurements did not, however, show evidence of the coherent oscillations in the time-resolved anisotropy that were seen in the calculations on isolated chromophore pairs. The surrounding medium undoubtedly plays a major role in destroying the coherences between exciton states that give rise to the oscillations seen in the calculations of Section 4. In this section, we include two aspects of the surrounding medium, namely, vibronic energy relaxation and dephasing, and examine their effects on the time-resolved anisotropy.

Our inclusion of vibrational relaxation and dephasing builds upon the approach of Jean, Friesner and Fleming. [26] In their work, Jean *et al.* developed a quantum mechanical theory of photo-induced electron transfer (see also the recent work of Pollard and Friesner on the application of Redfield theory to multilevel systems [27] and work by Walsh and Coalson [28]). Using Redfield relaxation theory, they incorporated vibrational relaxation through a coupling of the quantum-mechanical reaction coordinate of an electron transfer system to a thermal bath. We adopt a similar approach in our work, introducing a coupling of the intra-chromophore vibrations to a thermal bath.

In Section 5A, we derive the form of the time- and frequency-resolved signal in terms of the elements of the reduced chromophore pair density matrix. Then we introduce and describe the system-bath coupling operator in Section 5B. Section 5C explains some important details of our Redfield calculations, and results of numerical calculations of the time-resolved anisotropy including vibrational relaxation and dephasing are presented in Section 5D.

### 5A. Density Matrix Increment

In deriving a density matrix expression for the time- and frequency-resolved signal, the

notation of Section 4 will be used. In order to calculate the excited state population of the detector we need the contribution to the density matrix that is second order in the electric field of the excitation laser pulse and second order in the interaction with the detector. This contribution is given in the interaction picture by

$$\begin{aligned}\tilde{\rho}^{(4)}(t) = & \int_{t_0}^t d\tau \int_{t_0}^\tau d\tau_1 \int_{t_0}^{\tau_1} d\tau_2 \int_{t_0}^{\tau_2} d\tau_3 \{ \tilde{V}_d(\tau) \tilde{V}_e(\tau_1) \rho_0 \tilde{V}_e(\tau_3) \tilde{V}_d(\tau_2) \\ & + \tilde{V}_d(\tau) \tilde{V}_e(\tau_3) \rho_0 \tilde{V}_e(\tau_2) \tilde{V}_d(\tau_1) + \tilde{V}_d(\tau) \tilde{V}_e(\tau_2) \rho_0 \tilde{V}_e(\tau_3) \tilde{V}_d(\tau_1) + h.c.\},\end{aligned}\quad (55)$$

where  $\tilde{V}_d(t)$  and  $\tilde{V}_e(t)$  are the previously defined interaction Hamiltonians in the interaction picture, given by Eqs. (15) and (16), and  $\rho_0$  is the initial density matrix of the entire system, which is assumed initially to take the factorizable form

$$\rho_0 = \rho_{cp} \rho_b |a\rangle\langle a|. \quad (56)$$

$\rho_{cp} = |\alpha\rangle\langle\alpha|$  is the initial reduced density matrix of the chromophore pair and  $\rho_b$  is the initial density matrix of the thermal bath.  $H_0$  now includes the Hamiltonian of the thermal bath,  $H_b$ , and the chromophore pair-bath coupling,  $H_{bcp}$ , and is given by

$$H_0 = H_{cp} + H_d + H_b + H_{bcp}. \quad (57)$$

The precise form of  $H_{bcp}$  will be developed in Section 5B.

If the time  $t$  in Eq. (55) is large enough so that excitation and detection do not overlap, and the density matrix increment is defined as  $\Delta\tilde{\rho}^{(4)}(t)$  as

$$\Delta\tilde{\rho}^{(4)}(t) \equiv \tilde{\rho}^{(4)}(t + \frac{\Delta t}{2}) - \tilde{\rho}^{(4)}(t - \frac{\Delta t}{2}), \quad (58)$$

then the detected signal can be calculated with the help of

$$\Delta\tilde{\rho}^{(4)}(t) = \int_{t-\frac{\Delta t}{2}}^{t+\frac{\Delta t}{2}} d\tau \int_{t_0}^\tau d\tau_1 \int_{t_0}^\infty d\tau_2 \int_{t_0}^\infty d\tau_3 \tilde{V}_d(\tau) \tilde{V}_e(\tau_3) \rho_0 \tilde{V}_e(\tau_2) \tilde{V}_d(\tau_1) + h.c. \quad (59)$$

We arrive at Eq. (59) by noticing that when excitation and detection do not overlap, the first term on the right-hand side of Eq. (55) does not contribute to Eq. (59), and the upper limit of integration in the integral over  $\tau_2$  can be replaced by infinity.

The integrand in Eq. (59) can be simplified as follows. First, we make an assumption that the effects of the bath are negligible on the timescale of the duration of the laser pulse. That approximation allows us to neglect the system-bath coupling Hamiltonian in the terms  $\tilde{V}_e(\tau_3)$  and  $\tilde{V}_e(\tau_2)$ , and Eq. (59) becomes

$$\begin{aligned} \Delta\tilde{\rho}^{(4)}(t) \cong & \int_{t-\frac{\Delta t}{2}}^{t+\frac{\Delta t}{2}} d\tau \int_{t_0}^{\tau} d\tau_1 \frac{E_0^2}{4} \sum_{\gamma, \gamma'} \mu_{\alpha\gamma} \mu_{\alpha\gamma'} (\mathbf{e}_{\alpha\gamma} \cdot \mathbf{e}_L) (\mathbf{e}_{\alpha\gamma'} \cdot \mathbf{e}_L) \\ & \times F(\varepsilon_{\gamma\alpha} - \Omega) F(\varepsilon_{\gamma'\alpha} - \Omega) \tilde{V}_d(\tau) |\gamma\rangle\langle\gamma'| \rho_b |a\rangle\langle a| \tilde{V}_d(\tau_1) + h.c. \end{aligned} \quad (60)$$

where  $F(\varepsilon_{\gamma\alpha} - \Omega)$  has been previously defined by Eq. (54). We next write out explicitly the operators  $\tilde{V}_d(\tau)$  and  $\tilde{V}_d(\tau_1)$  in Eq. (60) and take the expectation value of  $\Delta\tilde{\rho}^{(4)}(t)$  in state  $|b\rangle|\alpha'\rangle$ . Since the Hamiltonian of the detector commutes with the rest of the operators in  $H_0$ , we replace  $H_d$  with the corresponding eigenenergy. Integrating the resulting expression over the frequency profile of the detector according to Eq. (20) yields

$$\begin{aligned} & \int_{-\infty}^{\infty} d\varepsilon_d D(\varepsilon_d - \bar{\varepsilon}_d) \langle b| \langle \alpha' | \Delta\tilde{\rho}^{(4)}(t) | \alpha' \rangle | b \rangle = \\ & \frac{E_0^2 \eta^2 \mu_d^2}{4} \sum_{\gamma, \gamma', \beta, \beta'} \mu_{\alpha\gamma} \mu_{\alpha\gamma'} \mu_{\alpha'\beta} \mu_{\alpha'\beta'} (\mathbf{e}_{\alpha\gamma} \cdot \mathbf{e}_L) (\mathbf{e}_{\alpha\gamma'} \cdot \mathbf{e}_L) (\mathbf{e}_{\alpha'\beta} \cdot \mathbf{e}_d) (\mathbf{e}_{\alpha'\beta'} \cdot \mathbf{e}_d) \\ & \times \int_{t-\frac{\Delta t}{2}}^{t+\frac{\Delta t}{2}} d\tau \int_{t_0}^{\tau} d\tau_1 F(\varepsilon_{\gamma\alpha} - \Omega) F(\varepsilon_{\gamma'\alpha} - \Omega) e^{i\bar{\varepsilon}_d(\tau-\tau_1)} e^{-(\tau-\tau_1)^2 \Delta^2/4} \\ & \times \langle \alpha' | e^{iH'_0\tau} | \alpha' \rangle \langle \beta | e^{-iH'_0\tau} | \gamma \rangle \langle \gamma' | \rho_b e^{iH'_0\tau_1} | \beta' \rangle \langle \alpha' | e^{-iH'_0\tau_1} | \alpha' \rangle + h.c., \end{aligned} \quad (61)$$

where  $D(\varepsilon_d - \bar{\varepsilon}_d)$  denotes the frequency window of the detector, given by Eq. (21), and the prime on  $H'_0$  indicates that  $H_d$  has been removed. At this stage we make a similar assumption regarding the coupling of the chromophore pair to the bath during detection as we made during the excitation pulse, namely, that the bath has a negligible effect on the chromophore pair on the timescale of the inverse of the frequency width of the detector,  $\Delta^{-1}$ . That assumption allows us to make the following approximate replacement in Eq. (61)

$$\langle \beta | e^{-iH'_0\tau} | \gamma \rangle \langle \gamma' | \rho_b e^{iH'_0\tau_1} | \beta' \rangle \cong \langle \beta | e^{-iH'_0\tau} | \gamma \rangle \langle \gamma' | \rho_b e^{iH'_0\tau} | \beta' \rangle e^{-i(H_b + E_{\beta'})(\tau - \tau_1)}. \quad (62)$$

Using Eq. (62) in Eq. (61) and taking the trace over the bath results in the final expression for the population of the state  $|\alpha'\rangle|b\rangle$ :

$$\begin{aligned}
Tr_b \left\{ \int_{-\infty}^{\infty} d\varepsilon_d D(\varepsilon_d - \bar{\varepsilon}_d) \langle b | \langle \alpha' | \Delta \tilde{\rho}^{(4)}(t) | \alpha' \rangle | b \rangle \right\} = \\
\frac{E_0^2 \eta^2}{4} \sum_{\gamma, \gamma', \beta, \beta'} \mu_{\alpha\gamma} \mu_{\alpha\gamma'} \mu_{\alpha'\beta} \mu_{\alpha'\beta'} (\mathbf{e}_{\alpha\gamma} \cdot \mathbf{e}_L) (\mathbf{e}_{\alpha\gamma'} \cdot \mathbf{e}_L) (\mathbf{e}_{\alpha'\beta} \cdot \mathbf{e}_d) (\mathbf{e}_{\alpha'\beta'} \cdot \mathbf{e}_d) \\
\times \int_{t-\frac{\Delta t}{2}}^{t+\frac{\Delta t}{2}} d\tau \int_{t_0}^{\tau} d\tau_1 F(\varepsilon_{\gamma\alpha} - \Omega) F(\varepsilon_{\gamma'\alpha} - \Omega) e^{-i(\varepsilon_{\beta'\alpha'} - \bar{\varepsilon}_d)(\tau - \tau_1)} e^{-(\tau - \tau_1)^2 \Delta^2 / 4} \\
\times Tr_b \{ \langle \beta | e^{-iH'_0\tau} | \gamma \rangle \langle \gamma' | \rho_b e^{iH'_0\tau} | \beta' \rangle \} + c.c. \quad (63)
\end{aligned}$$

Making approximations that neglect the effects of the bath during the excitation pulse and the detection time window confines the effects of the bath to  $Tr_b \{ \langle \beta | e^{-iH'_0\tau} | \gamma \rangle \langle \gamma' | \rho_b e^{iH'_0\tau} | \beta' \rangle \}$ . In order to evaluate the latter quantity we must now develop a model for the bath and the form of the bath-chromophore pair interaction.

## 5B. Bath-Chromophore Pair Interaction

Before proceeding farther, we make the following definition regarding the system and the bath. The degrees of freedom that we choose to treat explicitly are the two intra-chromophore modes, referred to as  $Q_1$  and  $Q_2$ . In general, we assume that any optically active collective coordinates (i.e. those whose equilibrium values are displaced in the excited electronic states) would be treated on the same explicit footing as  $Q_1$  and  $Q_2$ . Thus the bath modes are defined to be those collective coordinates that are not displaced when an optical transition takes place.

Consistently with our assumption of the factorizable form, Eq. (56) of the total initial density matrix in the electronic ground state, we neglect bath-chromophore pair interaction entirely prior to electronic excitation. We expand the system-bath coupling operator  $V_{eg}(Q_1, Q_2, q)$  for the singly excited state  $|eg\rangle$  about the equilibrium positions of  $Q_1$  and  $Q_2$  in that state, denoted by  $\Delta_1^{eg}$  and  $\Delta_2^{eg}$ , respectively, and let  $q$  denote the bath coordinates. Expanding  $V_{eg}(Q_1, Q_2, q)$  to first order in the displacement of  $Q_1$  and  $Q_2$  yields

$$\begin{aligned}
V_{eg}(Q_1, Q_2, q) \cong V_{eg}(\Delta_1^{eg}, \Delta_2^{eg}, q) + (Q_1 - \Delta_1^{eg}) \frac{\partial V_{eg}(\Delta_1^{eg}, \Delta_2^{eg}, q)}{\partial Q_1} + \\
(Q_2 - \Delta_2^{eg}) \frac{\partial V_{eg}(\Delta_1^{eg}, \Delta_2^{eg}, q)}{\partial Q_2}. \quad (64)
\end{aligned}$$

The  $q$ -dependence of the first term on the right-hand side of Eq. (64) would, in general,

contribute to optical dephasing. Considering  $q$  to be a single degree of freedom for purposes of illustration, we expand the first term on the right-hand-side of Eq. (64) in powers of  $q$  about its equilibrium position, which is chosen to be zero (and by definition, to be the same in the ground and both excited electronic states):

$$V_{eg}(\Delta_1^{eg}, \Delta_2^{eg}, q) \cong V_{eg}(\Delta_1^{eg}, \Delta_2^{eg}, 0) + \frac{q^2}{2} \frac{\partial^2 V_{eg}(\Delta_1^{eg}, \Delta_2^{eg}, 0)}{\partial q^2} + \dots \quad (65)$$

where the term linear in  $q$  vanishes. Terms quadratic, cubic, etc. in  $q$  represent changes in frequency, anharmonicity, etc. of that bath mode following optical excitation of chromophore 1. Because a collective coordinate of the type  $q$  will generally be of low frequency (long wavelength), its change in frequency, anharmonicity, etc. will be assumed to be negligibly small. The leading term in Eq. (64) is thereby taken to be sensibly  $q$ -independent as well as independent of the intramolecular coordinates; it can be absorbed into the nuclear Hamiltonian  $H_{eg}$ . Hence, we arrive at a working model in which all optically active collective coordinates are treated explicitly, the remaining (optically inactive) coordinates are relegated to the bath, and a phenomenological treatment of electronic dephasing need not be introduced. The remaining  $q$ -dependence in Eq. (64) resides in terms linear in  $(Q_1 - \Delta_1^{eg})$  and  $(Q_2 - \Delta_2^{eg})$ . These  $q$ -dependent terms govern bath-induced vibrational relaxation in the site state  $|eg\rangle$ .

In order to avoid unnecessary complications, we make an additional assumption that  $Q_1$  and  $Q_2$  couple to orthogonal combinations of bath coordinates, denoted by  $q_1$  and  $q_2$ , respectively. The system-bath coupling becomes

$$\begin{aligned} V_{eg}(Q_1, Q_2, q_1, q_2) &= V_{eg}^{(1)}(Q_1, q_1) + V_{eg}^{(2)}(Q_2, q_2) \\ &\cong (Q_1 - \Delta_1^{eg}) \frac{\partial V_{eg}^{(1)}(\Delta_1^{eg}, q_1)}{\partial Q_1} + (Q_2 - \Delta_2^{eg}) \frac{\partial V_{eg}^{(2)}(\Delta_2^{eg}, q_2)}{\partial Q_2}. \end{aligned} \quad (66)$$

There is an analogous expression for  $V_{ge}(Q_1, Q_2, q_1, q_2)$ . Since we are neglecting frequency shifts of the bath modes, it is consistent to make linear approximations to the derivatives in Eq. (66):

$$\frac{\partial V_{eg}^{(1)}(\Delta_1^{eg}, q_1)}{\partial Q_1} \cong q_1 \frac{\partial^2 V_{eg}^{(1)}(\Delta_1^{eg}, 0)}{\partial q_1 \partial Q_1} \equiv f_1 q_1 \quad (67)$$

and similarly for  $\frac{\partial V_{eg}^{(2)}(\Delta_2^{eg}, q_2)}{\partial Q_2}$ . In the end, assuming the bilinear coupling constants to be the same for both pairs of intramolecular and bath modes in both electronic excited states allows us to write simply

$$H_{bcp} = |eg\rangle\langle eg|\{(Q_1 - \Delta_1^{eg})f_l q_1 + (Q_2 - \Delta_2^{eg})f_l q_2)\} + |ge\rangle\langle ge|\{(Q_1 - \Delta_1^{ge})f_l q_1 + (Q_2 - \Delta_2^{ge})f_l q_2)\} . \quad (68)$$

In practice, we hold it that electronically exciting one chromophore leaves an intramolecular mode on the other undisplaced, so that  $\Delta_2^{eg} = \Delta_1^{ge} = 0$ .

### 5C. Vibronic Relaxation

In Eq. (63) for the detector-frequency-weighted populations in the states  $|\alpha'\rangle|b\rangle$ , the effects of the bath have been confined to the terms  $Tr_b\{\langle\beta|e^{-iH'_0\tau}|\gamma\rangle\langle\gamma'|\rho_b e^{iH'_0\tau}|\beta'\rangle\}$ , which is the  $\beta\beta'^{th}$  element of the reduced chromophore pair operator  $\sigma(t)$  obtained by propagating  $\sigma(0) \equiv |\gamma\rangle\langle\gamma'|\rho_b$  under  $H'_0$  and tracing over the bath. It is convenient to propagate the elements of the initial density matrix of the system term by term in order to facilitate the orientational averaging. Since the system-bath coupling is assumed to be weak, we can follow the recent work of Jean and co-workers and use Redfield theory to calculate the time development of the operators  $\sigma(t)$ .

Since Redfield theory is most naturally implemented here in the exciton (i.e. eigenstate) representation of the chromophore pair Hamiltonian, the system-bath coupling must be transformed from the site representation, in which the matrix elements of  $H_{bcp}$ , Eq. (68), between site vibrational quantum number states are readily calculated, to the exciton representation. The system-bath coupling in the exciton representation connects various exciton states and ultimately leads to population and phase relaxation among the exciton states.

The Redfield equations of motion for the reduced operators  $\sigma(t)$  have the form [26,27,29]

$$\dot{\sigma}_{\beta\beta'}(t) = -i\varepsilon_{\beta\beta'}\sigma_{\beta\beta'}(t) + \sum_{\kappa,\kappa'} R_{\beta\beta',\kappa\kappa'} \sigma_{\kappa\kappa'}(t) \quad (69)$$

and the Redfield tensor  $R_{\beta\beta',\kappa\kappa'}$  is specified by

$$\begin{aligned}
R_{\beta\beta',\kappa\kappa'} &= \int_0^\infty dt \{ \langle [H_{bcp}(t)]_{\kappa'\beta'} [H_{bcp}(0)]_{\beta\kappa} \rangle e^{i\varepsilon_{\kappa\beta} t} + \langle [H_{bcp}(0)]_{\kappa'\beta'} [H_{bcp}(t)]_{\beta\kappa} \rangle e^{i\varepsilon_{\beta'\kappa'} t} \\
&\quad - \delta_{\kappa'\beta'} \sum_\xi \langle [H_{bcp}(t)]_{\beta\xi} [H_{bcp}(0)]_{\xi\kappa} \rangle e^{i\varepsilon_{\kappa\xi} t} - \delta_{\kappa\beta} \sum_\xi \langle [H_{bcp}(0)]_{\kappa'\xi} [H_{bcp}(t)]_{\xi\beta'} \rangle e^{i\varepsilon_{\xi\kappa'} t} \}
\end{aligned} \quad (70)$$

where  $[H_{bcp}(t)]_{\beta\kappa} \equiv e^{iH_b t} [H_{bcp}]_{\beta\kappa} e^{-iH_b t}$  and  $\langle \dots \rangle \equiv Tr_b \{ \dots \rho_b \}$ .

The bath-chromophore pair interaction in Eq. (68) is a sum of products of chromophore pair and bath operators, and the transformation of the system-bath coupling operator to the exciton representation leaves the bath operators untouched. Therefore, bath-chromophore pair interactions in the exciton representation can readily be expressed as a sum of products of chromophore pair and bath operators, and we adopt Pollard and Friesner's notation for the Redfield tensor which is appropriate to such a form [27]

$$\begin{aligned}
R_{\beta\beta',\kappa\kappa'} &= \sum_{a=1}^2 [(G_a)_{\kappa'\beta'} (G_a)_{\beta\kappa} \{ (\Theta_{aa}^+)_\beta + (\Theta_{aa}^-)_{\kappa'\beta'} \} \\
&\quad - \delta_{\kappa'\beta'} \sum_\xi (G_a)_{\beta\xi} (G_a)_{\xi\kappa} (\Theta_{aa}^+)_\xi - \delta_{\beta\kappa} \sum_\xi (G_a)_{\kappa'\xi} (G_a)_{\xi\beta'} (\Theta_{aa}^-)_{\kappa'\xi} ] ,
\end{aligned} \quad (71)$$

where (see Eq. (68))

$$\begin{aligned}
G_1 &= |eg\rangle\langle eg| (Q_1 - \Delta_1^{eg}) f_l + |ge\rangle\langle ge| Q_1 f_l \\
G_2 &= |eg\rangle\langle eg| Q_2 f_l + |ge\rangle\langle ge| (Q_2 - \Delta_2^{ge}) f_l ,
\end{aligned} \quad (72)$$

and  $(\Theta_{aa}^\pm)_{\beta\delta}$  are given by

$$(\Theta_{aa}^\pm)_{\beta\delta} = \int_0^\infty d\tau e^{-i\varepsilon_{\beta\delta}\tau} \langle q_a(\pm\tau) q_a \rangle . \quad (73)$$

The expression for the Redfield tensor given by Pollard and Friesner [27] also includes contributions from cross-correlations of different sets of bath coordinates, but since we assume that  $q_1$  and  $q_2$  are completely uncorrelated, the terms involving cross-correlations between  $q_1$  and  $q_2$  vanish.

Neglecting the imaginary part of  $(\Theta_{aa}^\pm)_{\beta\delta}$ , Eq. (73) can be rewritten as

$$(\Theta_{aa}^\pm)_{\beta\delta} \cong \frac{1}{2} \int_{-\infty}^\infty d\tau e^{-i\varepsilon_{\beta\delta}\tau} \langle q_a(\pm\tau) q_a \rangle \quad (74)$$

$$\cong e^{\mp\beta\varepsilon_{\beta\delta}\tau} \frac{1}{2} \int_{-\infty}^\infty d\tau e^{-i\varepsilon_{\beta\delta}\tau} \langle q_a q_a(\pm\tau) \rangle . \quad (75)$$

Equations (74) and (75) can be combined to obtain  $(\Theta_{aa}^\pm)_{\beta\delta}$  in terms of the symmetrized correlation function,

$$(\Theta_{aa}^\pm)_{\beta\delta} = \frac{1}{1 + e^{\pm\beta\varepsilon_{\beta\delta}}} \int_{-\infty}^{\infty} d\tau e^{-i\varepsilon_{\beta\delta}\tau} \frac{1}{2} \{ \langle q_a q_a(\pm\tau) \rangle + \langle q_a(\pm\tau) q_a \rangle \}, \quad (76)$$

Pollard and Friesner have emphasized that whatever its shortcomings, the neglect of the imaginary part of  $(\Theta_{aa}^\pm)_{\beta\delta}$  does not undermine detailed balance. In fact, the symmetrized correlation function in Eq. (76) can be replaced by any approximate function that is real and even with respect to time. We introduce a mean-squared fluctuation and bath correlation time by hypothesizing that

$$\frac{1}{2} (\langle q_a q_a(\pm\tau) \rangle + \langle q_a(\pm\tau) q_a \rangle) = \langle q_a^2 \rangle e^{-|\tau|/\tau_c}, \quad (77)$$

Using Eq. (77) in Eq. (76) leads to

$$\begin{aligned} (\Theta_{aa}^\pm)_{\beta\delta} &\cong \frac{1}{1 + e^{\pm\beta\varepsilon_{\beta\delta}}} \int_{-\infty}^{\infty} d\tau e^{-i\varepsilon_{\beta\delta}\tau} \langle q_a^2 \rangle e^{-|\tau|/\tau_c} \\ &\cong \frac{1}{1 + e^{\pm\beta\varepsilon_{\beta\delta}}} \cdot \frac{2/\tau_c}{1/\tau_c^2 + \varepsilon_{\beta\delta}^2} \langle q_a^2 \rangle. \end{aligned} \quad (78)$$

When  $\tau_c$  is short compared to all relevant bohr periods in the system, we obtain

$$(\Theta_{aa}^\pm)_{\beta\delta} = \frac{1}{1 + e^{\pm\beta\varepsilon_{\beta\delta}}} (2\tau_c \langle q_a^2 \rangle). \quad (79)$$

This panoply of assumptions and approximations allows us to specify the entire Redfield tensor by choosing a single parameter. [27] In the absence of excitation transfer, the Redfield tensor element governing the rate of population decay from  $|eg\rangle|1_e 0_g\rangle$  ( $\equiv |1\rangle$ ) to  $|eg\rangle|0_e 0_g\rangle$  ( $\equiv |0\rangle$ ) is

$$R_{00,11} = (G_1)_{10}(G_1)_{01} \left\{ \frac{2}{1 + e^{-\beta\omega}} \cdot 2\tau_c \langle q_1^2 \rangle \right\}, \quad (80)$$

where  $(G_1)_{10} = (G_1)_{01} = f_l/\sqrt{2\omega}$ , and we can therefore choose the product of  $f_l^2$  and  $\tau_c \langle q_1^2 \rangle$  that yields a specified vibrational population decay rate from  $|eg\rangle|1_e 0_g\rangle$  to  $|eg\rangle|0_e 0_g\rangle$ .

In our calculations we make the secular approximation, namely, we keep only those elements of the Redfield tensor  $R_{\beta\beta',\kappa\kappa'}$  in which the element is not significantly smaller than the frequency mismatch  $|\omega_{\beta\beta'} - \omega_{\kappa\kappa'}|$ .

## 5D. Anisotropy Decays

Figure 7 shows calculated anisotropies for a chromophore pair with molecular parameters, laser pulse duration, and detector time and frequency resolution all the same as those used for the calculations of Figure 1. The initial state of the chromophore pair is  $|gg\rangle|0_g0_g\rangle$  and the bath is at 300 K. The population relaxation rate (in the absence of energy transfer) from  $|eg\rangle|1_e0_g\rangle$  to  $|eg\rangle|0_e0_g\rangle$  is chosen to be  $1.5 \text{ ps}^{-1}$  and for times less than 150 fs (overlapping laser pulse and detection window) the dissipative effects of the bath are not included. This is done in order to properly include the contributions to the fluorescence rate present when the excitation pulse and the detection window overlap. We combine the instantaneous fluorescence rate obtained from an isolated chromophore pair for times less than 150 fs with the rate including dissipation for times longer than 150 fs. The combined rate is then integrated and used to calculate the time-resolved signal. Since the combined rate is composed of two different calculations, there is a discontinuity in the combined rate, leading to a slight discontinuity in the slope of the short-time anisotropy.

The dissipative effects of the bath become most evident after about 0.75 ps, where the calculated anisotropies in Figures 1 and 7 cease to resemble each other. After 1.5 ps, the absence of oscillations in the time-resolved anisotropies of Figure 7 suggests that the coherences between the exciton states are almost completely destroyed by the bath, and the slow decay of the anisotropies beyond 1.5 ps results from the populations in the reduced density matrix of the chromophore pair approaching their equilibrium values at 300 K. Our claim that the slow monotonic decay of the time-resolved anisotropies beyond 1.5 ps is due to the thermal equilibration of populations is supported by the calculations of the site excitation probability presented below. The lower (thin) curve in Figure 7 shows a more significant decay in the 1.5-4 ps region than the upper (thick) curve because the excitation conditions that result in the anisotropy shown by the lower (thin) curve prepare a higher-lying superposition of states that subsequently decays into states localized on (the lower-energy) chromophore 1. Excitation conditions resulting in the anisotropy shown by the upper (thick) curve prepare a superposition of states fairly well localized on the lower-

energy chromophore, and therefore, population relaxation does not result in a significant decay of the anisotropy in the 2-4 ps region.

Figure 8 presents a calculation of the time-resolved anisotropy designed to check whether the time-resolved anisotropy behaves in a qualitatively similar manner when higher-lying thermally populated initial ground states are included. The contributions from the lowest three thermally populated levels  $|gg\rangle|0_g0_g\rangle$ ,  $|gg\rangle|1_g0_g\rangle$ , and  $|gg\rangle|0_g1_g\rangle$  have been included in Figure 8. The contributions to the anisotropy from  $|gg\rangle|1_g0_g\rangle$  and  $|gg\rangle|0_g1_g\rangle$  are qualitatively similar to the  $|gg\rangle|0_g0_g\rangle$ , and calculated anisotropies in Figure 8 show a similar behavior to those shown in Figure 7. In the case of excitation  $100\text{ cm}^{-1}$  above the zero-zero transition frequency of the higher-energy chromophore, there is a perceptible smoothing of the coherent oscillations at early times, compared to its counterpart in Figure 7.

The initial anisotropy in Fig. 8 still remains above 0.4 even with the inclusion of higher-lying thermally populated initial ground states. For example, consider the initial state  $|gg\rangle|1_g0_g\rangle$ . The short-time excitation is dominated by the strongest Franck-Condon transitions and occurs to the states  $|ge\rangle|1_g0_e\rangle$  and  $|eg\rangle|1_e0_g\rangle$ . (Recall that for very short delays both the excitation pulse and the detection window are effectively shortened, increasing their effective bandwidths.) Because each of these singly-excited states involves excitation on a different chromophore, the emission from these states back to  $|gg\rangle|1_g0_g\rangle$  is the type that leads to a larger than 0.4 initial anisotropy.

Figure 9 shows a calculation of the time-resolved anisotropy, including vibrational relaxation, for the same case of a pair of identical chromophores and the same excitation and detection parameters used in Figure 4. The vibrational population decay rate of  $1.5\text{ ps}^{-1}$  from  $|eg\rangle|1_e0_g\rangle$  to  $|eg\rangle|0_e0_g\rangle$  in the absence of energy transfer was again used in this calculation. The overall qualitative behavior of the two anisotropy curves is in some ways similar to their counterparts in Figure 7. However, the slow decay in the 2-4 ps range seen in the anisotropy curves in Figure 7 is absent in the corresponding curves in Figure 9. This is consistent with the fact that there can be no net population transfer between two identical chromophores.

The net site excitation probability difference  $P_1(t) - P_2(t)$ , given by Eq. (53) for the case of the isolated chromophore pair, can also be calculated with the inclusion of dissipative effects of the bath. The net site population difference can be written in terms of the reduced density matrix of the chromophore pair

$$P_1(t) - P_2(t) = \text{Tr}_{cp}\{(P_1 - P_2)\text{Tr}_b\{e^{-iH'_0 t}\rho_{cp}(0)e^{iH'_0 t}\}\}, \quad (81)$$

where  $H'_0 = H_{cp} + H_b + H_{bcp}$ , and  $\text{Tr}_{cp}\{\dots\}$  denotes the trace over the states of the chromophore pair. The initial density matrix of the chromophore pair, neglecting the effects of the bath during the excitation pulse, is given by

$$\rho_{cp}(0) = \sum_{\gamma, \gamma'} |\gamma\rangle\langle\gamma'| \mu_{\alpha\gamma} \mu_{\alpha\gamma'} \overline{(\mathbf{e}_{\alpha\gamma} \cdot \mathbf{e}_L)(\mathbf{e}_{\alpha\gamma'} \cdot \mathbf{e}_L)} F(\varepsilon_{\gamma\alpha} - \Omega) F(\varepsilon_{\gamma'\alpha} - \Omega) \quad (82)$$

Calculation of  $P_1(t) - P_2(t)$  for the system parameters and excitation conditions identical to those used for obtaining the anisotropies in Figure 7 are shown in Figure 10. The upper (thick) curve in Figure 10 is initially similar to the thick curve in Figure 6a, where the effects of the bath were not included.  $P_1(t) - P_2(t)$  for the isolated chromophore pair is oscillatory but remains close to its initial value. When the bath is included, the oscillations are damped out and the excitation probability difference tends to its equilibrium value. The behavior of the excitation probability difference shown by the lower (thin) curve of Figure 10 is even more dramatic. The large oscillations present in its analog in Figure 6b are completely damped out by 2 ps, indicating that coherent net population transfer has stopped. Both curves in Figure 10 approach the same steady-state value of 0.34, consistent with thermal equilibration at 300 K.

## 6. CONCLUSIONS

We have presented calculations of time-resolved fluorescence anisotropy from a chromophore pair undergoing excitation transfer following excitation with an ultrashort laser pulse. An intramolecular mode for each chromophore was explicitly included in our model,

in order to understand the effects of vibrational structure on the anisotropy. We have included a model detector in order to take realistic account of the limitations imposed by the time and frequency resolution of the experimental detection process.

Choosing parameters for our model system to correspond to the degree possible to known parameters in closely-coupled chromophore pairs in C-PC, we have investigated the excitation wavelength dependence of the time-resolved anisotropy, observing behavior qualitatively similar to the experimental findings. [4] Also, using a simplified version of our model that can be treated analytically, we have shown that the initial values of the anisotropy are highly dependent on the ground state(s) into which the chromophore is emitting.

The inclusion of vibrational structure is shown to play a major role in determining the form of the time-resolved anisotropy. Several effects are observed that are not present if each chromophore is treated as an electronic 2-level system without nuclear degrees of freedom. First, the presence of multiple vibrational levels in the excited state of each chromophore introduces excitation-wavelength dependence that is significantly different from that found in a pair of coupled two-level systems. Second, in a chromophore pair lacking vibrational structure, coherent energy transfer requires a pulse bandwidth in excess of the bare exciton splitting, which is greater than the site energy difference. On the other hand, when each chromophore has a ladder of excited vibronic states, preparation of a superposition of close-lying vibronic states with amplitude on both chromophores can sometimes be accomplished with a pulse bandwidth less than the difference between the two sites in zero-zero transition frequency. Finally, the vibrational levels in the ground electronic state selected by the detection bandwidth play a significant role in determining the effects of quantum mechanical interference on the time-resolved anisotropy.

We have reported Redfield theory calculations of the anisotropy, which included coupling of the intramolecular coordinates to a surrounding medium. When the effects of a thermal bath were included, the coherent oscillations in the anisotropy remained at short times but were seen to decay prior to the anisotropy reaching its steady-state value. It is interesting to note, however, that evidence for the coherent oscillations, which are present

in our calculations including vibronic relaxation, seems to be lacking in the experimental anisotropies measured for APC and C-PC by Xie *et al.* [4] Failure to sum over all vibrational levels initially thermally populated at 300 K causes the coherent oscillations in the anisotropy to be exaggerated. It can also be anticipated that addition of multiple optically active intramolecular and/or collective modes would tend to obscure the oscillatory contribution to the calculated signals. Furthermore, the coherent oscillations in the anisotropy can be degraded by the presence of inhomogeneous broadening in the zero-zero frequency offset between the two chromophores. Even if the zero-zero transition energies in the two chromophores are perfectly correlated, the inhomogeneous broadening of the zero-zero transition energies will have the effect of creating a distribution of different excitation and detection conditions, which could also tend to mask the coherent anisotropy oscillations.

In very recent work, Jean [30] has reported calculations on fluorescence emission from an electron transfer system including vibronic relaxation via Redfield theory and a treatment of the frequency-dependent instantaneous emission rate essentially equivalent to our model detection apparatus. He reports the interesting result that under some circumstances, the instantaneous emission rate can accurately reflect the extent of electron transfer.

## ACKNOWLEDGMENTS

We thank Sunney Xie, Mei Du, and Graham Fleming for many helpful discussions and suggestions. We also thank John Jean and Eric Hiller for their advice regarding the implementation of Redfield theory, and Lowell Ungar, Tim Smith, Stephen Bradforth and Sandy Rosenthal for their comments on the manuscript. This work was supported by the National Science Foundation and the Camille and Henry Dreyfus Teacher-Scholar Award Program.

## APPENDIX: ORIENTATIONAL AVERAGING

We need to obtain the average over the products of four direction cosines in Eq. (31), where  $\mathbf{e}_+$  and  $\mathbf{e}_-$  are unit vectors in the molecule-fixed frame,  $\mathbf{e}_L$  and  $\mathbf{e}_d$  are unit vectors in

the laboratory-fixed frame, and there is a constant relative angle  $\gamma$  maintained between  $\mathbf{e}_+$  and  $\mathbf{e}_-$ . The averages of the first two products in Eq. (31) are [31]

$$\begin{aligned}\overline{(\mathbf{e}_\pm \cdot \mathbf{e}_L)^2 (\mathbf{e}_\pm \cdot \mathbf{e}_d)^2} &= \frac{1}{5} \text{ for } \mathbf{e}_L \parallel \mathbf{e}_d \\ &= \frac{1}{15} \text{ for } \mathbf{e}_L \perp \mathbf{e}_d.\end{aligned}\quad (83)$$

The average over the crossterm  $(\mathbf{e}_+ \cdot \mathbf{e}_L)(\mathbf{e}_- \cdot \mathbf{e}_L)(\mathbf{e}_+ \cdot \mathbf{e}_d)(\mathbf{e}_- \cdot \mathbf{e}_d)$  can be calculated by expressing  $\mathbf{e}_-$  in terms of  $\mathbf{e}_+$  and  $\mathbf{e}_{+\perp}$ , a vector perpendicular to  $\mathbf{e}_+$

$$\mathbf{e}_- = \mathbf{e}_+ \cos \gamma + \mathbf{e}_{+\perp} \sin \gamma. \quad (84)$$

Substituting Eq. (84) for  $\mathbf{e}_-$  enables us to express the above product as a sum of products where the molecule-fixed unit vectors are either parallel or perpendicular to each other. The average can then be calculated to give [31]

$$\begin{aligned}\overline{(\mathbf{e}_+ \cdot \mathbf{e}_L)(\mathbf{e}_- \cdot \mathbf{e}_L)(\mathbf{e}_+ \cdot \mathbf{e}_d)(\mathbf{e}_- \cdot \mathbf{e}_d)} &= \frac{1}{5} \cos^2 \gamma + \frac{1}{15} \sin^2 \gamma \text{ for } \mathbf{e}_L \parallel \mathbf{e}_d \\ &= \frac{1}{15} \cos^2 \gamma - \frac{1}{30} \sin^2 \gamma \text{ for } \mathbf{e}_L \perp \mathbf{e}_d.\end{aligned}\quad (85)$$

Eq. (38) is obtained by noting that for the case of identical chromophores, we have  $\mu_1 = \mu_2 \equiv \mu$  and  $\mathbf{e}_+ \perp \mathbf{e}_-$ , (i.e.  $\gamma = \pi/2$ ). Therefore, using Eq. (36), we can write

$$\mu_\pm^2 = \mu^2 \langle 0_g 0_g | 0_e 0_g \rangle^2 (1 \pm \mathbf{e}_1 \cdot \mathbf{e}_2). \quad (86)$$

Defining  $\cos \phi \equiv \mathbf{e}_1 \cdot \mathbf{e}_2$ , and substituting Eq. (86) into Eq. (37), Eq. (38) is obtained.

The orientational averages required for the evaluation of Eqs. (49) and (63) can be similarly evaluated by writing

$$\mathbf{e}_2 = \mathbf{e}_1 \cos \phi + \mathbf{e}_{1\perp} \sin \phi, \quad (87)$$

which makes it possible to express all orientational averages in terms of products of averages involving only parallel or perpendicular unit vectors in the molecule-fixed frame. The averages needed in Eqs. (49) and (63) are

$$\begin{aligned}\overline{(\mathbf{e}_{1(2)} \cdot \mathbf{e}_L)^2 (\mathbf{e}_{1(2)} \cdot \mathbf{e}_d)^2} &= \frac{1}{5} \text{ for } \mathbf{e}_L \parallel \mathbf{e}_d \\ &= \frac{1}{15} \text{ for } \mathbf{e}_L \perp \mathbf{e}_d ,\end{aligned}$$

$$\begin{aligned}\overline{(\mathbf{e}_{2(1)} \cdot \mathbf{e}_L)^2 (\mathbf{e}_{1(2)} \cdot \mathbf{e}_d)^2} &= \frac{1}{5} \cos^2 \phi + \frac{1}{15} \sin^2 \phi \text{ for } \mathbf{e}_L \parallel \mathbf{e}_d \\ &= \frac{1}{15} \cos^2 \phi + \frac{2}{15} \sin^2 \phi \text{ for } \mathbf{e}_L \perp \mathbf{e}_d ,\end{aligned}$$

$$\begin{aligned}\overline{(\mathbf{e}_{2(1)} \cdot \mathbf{e}_L)(\mathbf{e}_{1(2)} \cdot \mathbf{e}_L)(\mathbf{e}_{1(2)} \cdot \mathbf{e}_d)(\mathbf{e}_{2(1)} \cdot \mathbf{e}_d)} &= \frac{1}{5} \cos^2 \phi + \frac{1}{15} \sin^2 \phi \text{ for } \mathbf{e}_L \parallel \mathbf{e}_d \\ &= \frac{1}{15} \cos^2 \phi - \frac{1}{30} \sin^2 \phi \text{ for } \mathbf{e}_L \perp \mathbf{e}_d ,\end{aligned}$$

and

$$\begin{aligned}\overline{(\mathbf{e}_{2(1)} \cdot \mathbf{e}_L)^2 (\mathbf{e}_{1(2)} \cdot \mathbf{e}_d)(\mathbf{e}_{2(1)} \cdot \mathbf{e}_d)} &= \frac{1}{5} \cos \phi \text{ for } \mathbf{e}_L \parallel \mathbf{e}_d \\ &= \frac{1}{15} \cos \phi \text{ for } \mathbf{e}_L \perp \mathbf{e}_d ,\end{aligned}\tag{88}$$

## REFERENCES

- [1] R. Silbey, *Ann. Rev. Phys. Chem.* **27**, 203 (1976).
- [2] G. R. Fleming and R. van Grondelle, *Physics Today* **47**, no. 2, 48 (1994).
- [3] S. Rackovsky and R. Silbey, *Molec. Phys.* **25**, 61 (1973).
- [4] X. Xie, M. Du, L. Mets and G. R. Fleming, *Time-Resolved Laser Spectroscopy in Biochemistry III* SPIE **1640**, 690 (1992).
- [5] T. Schirmer, W. Bode, and R. Huber, *J. Mol. Biol.* **196**, 677 (1987), M. Duerring, G. B. Schmidt and R. Huber, *J. Mol. Biol.* **217**, 577 (1991).
- [6] W. F. Beck and K. Sauer, *J. Phys. Chem.* **96**, 4658 (1992).
- [7] T. Gillbro, A. V. Sharkov, I. V. Kryukov, E. V. Khoroshilov, P. G. Kryukov, R. Fischer and H. Scheer, *Biochim. Biophys. Acta* **1140**, 321 (1992).
- [8] Y. R. Kim, P. Share, M. Pereira, M Sarisky and R. M. Hochstrasser, *J. Chem. Phys.* **91**, 7557 (1989).
- [9] F. Zhu, C. Galli and R. M. Hochstrasser, *J. Chem. Phys.* **98**, 1042 (1993), *ibid.*, **98**, 9222 (1993).
- [10] K. Wynne, S. Gnanakaran, C. Galli, F. Zhu and R. M. Hochstrasser, *J. Lumin.* **60&61**, 735 (1994).
- [11] C. Galli, K. Wynne, S. M. LeCours, M. J. Therein and R. M. Hochstrasser, *Chem. Phys. Lett.* **206**, 493 (1993).
- [12] K. Wynne and R. M. Hochstrasser, *Chem. Phys.* **171**, 179 (1993), *ibid.* **173**, 539 (1993).
- [13] R. S. Knox and D. Gülen, *Photochem. Photobiol.* **57**, 40 (1993).
- [14] T. Förster in *Modern Quantum Chemistry*, Vol. III, p. 93, ed. by O. Sinanoglu, (Academic Press, New York, 1965).

[15] T. S. Rahman, R. S. Knox and V. M. Kenkre, *Chem. Phys.* **44**, 197 (1979), *ibid.* **47**, 416 (1980). For a theoretical study of quantum beats in time-resolved total emission from a dimer, see D. M. Burland and A. H. Zewail, *Adv. Chem. Phys.* **XL**, 369 (1979).

[16] T. J. Smith, L. W. Ungar and J. A. Cina, *J. Lumin.* **58**, 66 (1994).

[17] M. Chachisvilis, T. Pullerits, M. R. Jones, C. N. Hunter and V. Sundström, *Chem. Phys. Lett.* **224**, 345 (1994).

[18] T. Pullerits, M. Chachisvilis, M. R. Jones, C. N. Hunter and V. Sundström, *Chem. Phys. Lett.* **224**, 355 (1994).

[19] S. Bradforth, R. Jimenez, V. Fidler, G. Fleming, S. Nagarajan, J. Norris, F. van Mourik and R. van Grondelle, *Ultrafast Phenomena*, 1994 Technical Digest, p. 594.

[20] The vibrational modes in our model are assumed to be totally symmetric. If these modes were not totally symmetric, the vibronic selection rules would introduce complications in absorption, emission and ultimately, in the anisotropy.

[21] L. W. Ungar and J. A. Cina, work in progress, use a slightly different detection scheme in calculations on fluorescence upconversion measurements in solvation dynamics. In those calculations, the detector consists of *three* level systems within which two-photon transitions are made under the combined influence of the radiating molecule and a transform-limited gate pulse. In that scheme, the gate pulse directly provides both temporal and frequency resolution. See J. S. Melinger and A. C. Albrecht, *J. Chem. Phys.* **84**, 1247 (1986) for a detailed discussion of time and frequency resolution in light-induced emission.

[22] X. Xie, private communication.

[23] C. Cohen-Tannoudji, B. Diu and F. Laloë, *Quantum Mechanics*, p. 420, (Wiley-Interscience, New York, 1977).

- [24] K. Sauer and H. Scheer, *Biochim. Biophys. Acta.* **936**, 157 (1988).
- [25] K. Sauer, H. Scheer and P. Sauer, *Photochem. Photobiol.* **46**, 427 (1987).
- [26] J. M. Jean, R. A. Friesner and G. R. Fleming, *J. Chem. Phys.* **96**, 5827 (1992).
- [27] W. T. Pollard and R. A. Frienser, *J. Chem. Phys.* **100**, 5054 (1994).
- [28] A. M. Walsh and R. D. Coalson, *Chem. Phys. Lett.* **198**, 293 (1992).
- [29] R. Wertheimer and R. Silbey, *Chem. Phys. Lett.* **75**, 243 (1980).
- [30] J. M. Jean, *J. Chem. Phys.* submitted.
- [31] R. N. Zare, *Angular Momentum* (Wiley-Interscience, New York, 1988).

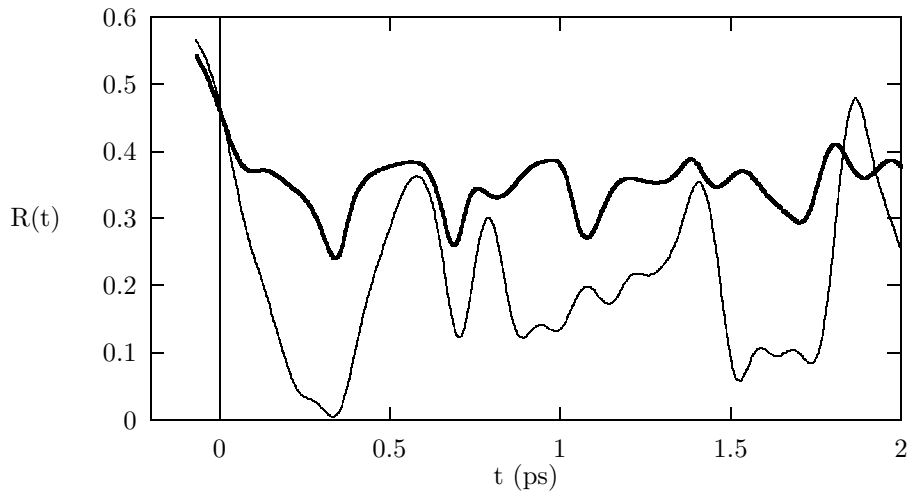


Figure 1. Time-resolved anisotropy plots for two different excitation/detection conditions. Upper (thick) curve corresponds to excitation at zero-zero transition frequency of lower-energy chromophore, lower (thin) curve is for excitation  $100 \text{ cm}^{-1}$  above the zero-zero transition frequency of higher-energy chromophore. Detector, with a time window of 70 fs, is red-shifted from excitation by  $250 \text{ cm}^{-1}$ .

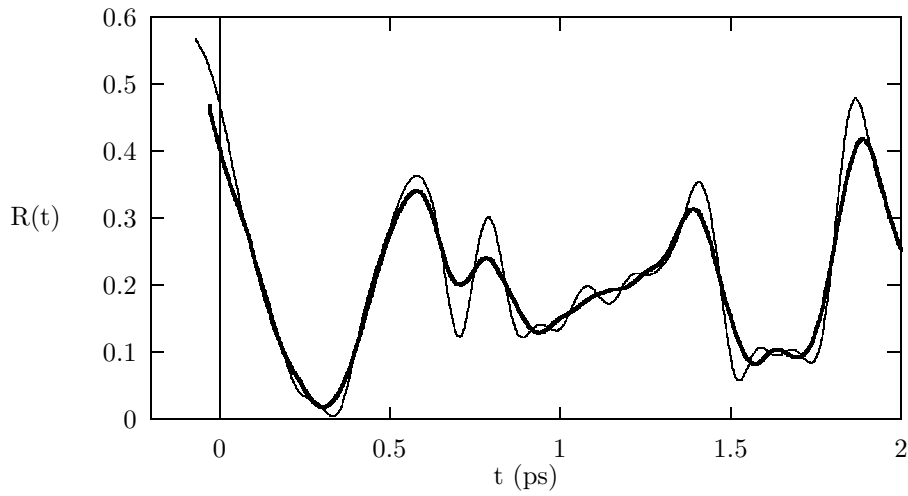


Figure 2. Time-resolved anisotropy corresponding to excitation at  $100 \text{ cm}^{-1}$  above zero-zero transition frequency of higher-energy chromophore. Thin curve results from time detection window of 70 fs (same as in Fig. 1), and thick curve is for a time detection window of 150 fs.

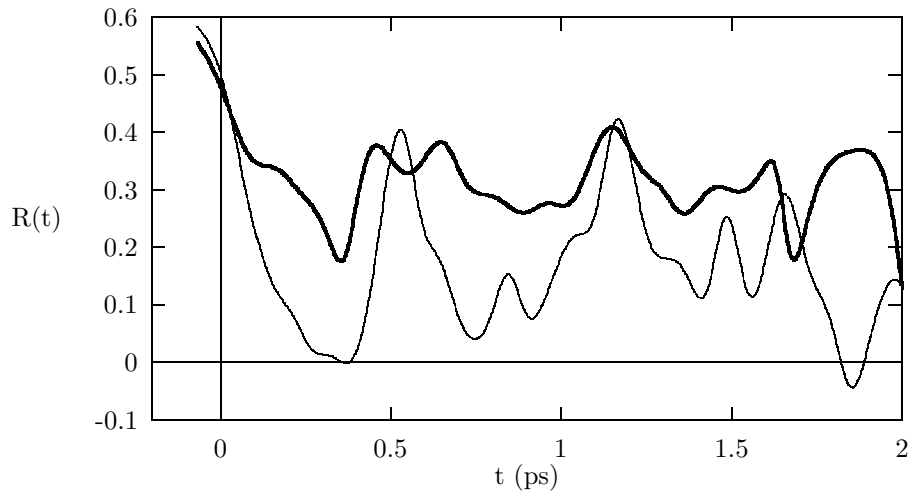


Figure 3. Time-resolved anisotropy for chromophore pair with  $100\text{ cm}^{-1}$  difference between the zero-zero electronic transition frequencies. Upper (thick) curve corresponds to excitation at zero-zero transition frequency of lower-energy chromophore, lower (thin) curve is for excitation  $150\text{ cm}^{-1}$  above the zero-zero transition frequency of higher-energy chromophore.

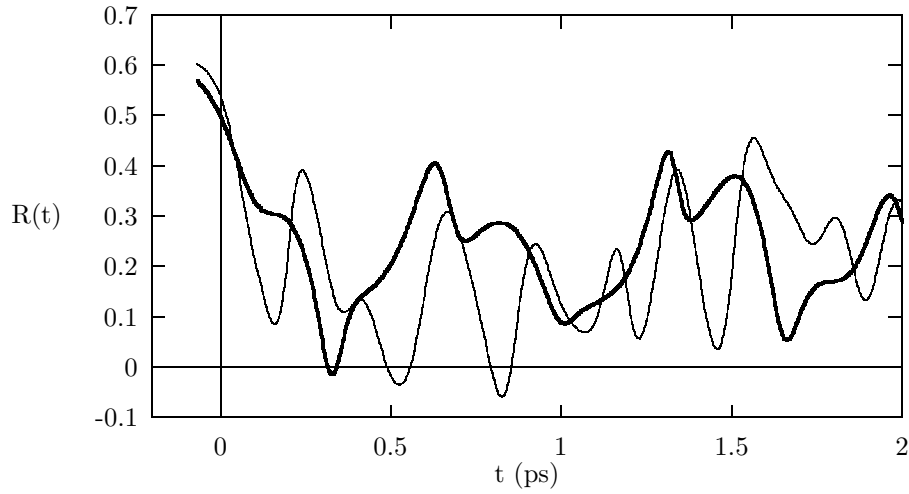


Figure 4. Time-resolved anisotropy for a pair of identical chromophores. Upper (thick) curve corresponds to excitation at zero-zero transition frequency of the chromophores, lower (thin) curve corresponds to excitation  $250\text{ cm}^{-1}$  above the zero-zero transition frequency.

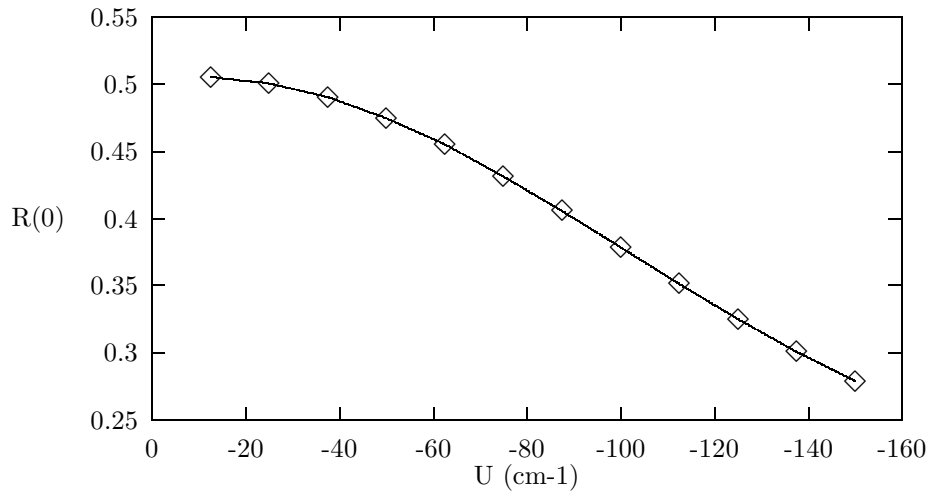


Figure 5. Anisotropy at  $t = 0$  as a function of excitation transfer coupling. Excitation/detection conditions and model system parameters are the same as in the lower (thin) curve of Figure 1.

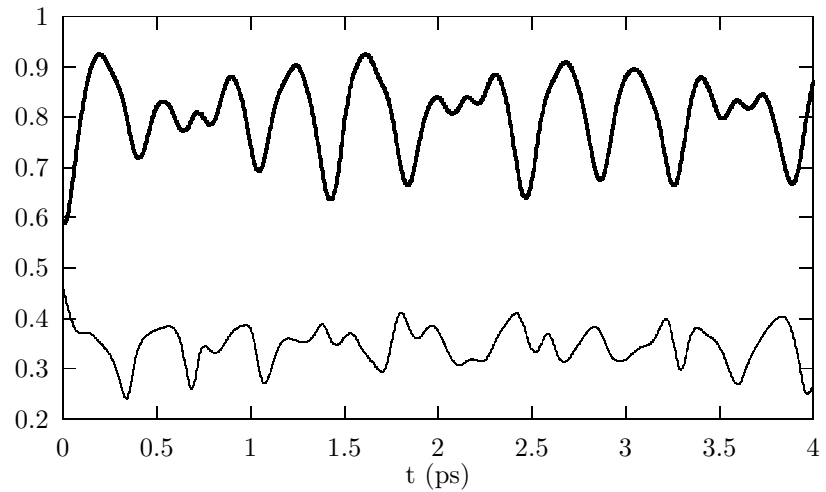


Figure 6a. Thick curve shows the site population difference obtained with same system parameters and excitation conditions as in the upper (thick) curve of Fig. 1. The thin curve shows the corresponding anisotropy. Both  $\frac{P_1(t) - P_2(t)}{P_1(t) + P_2(t)}$  and  $R(t)$  are dimensionless.

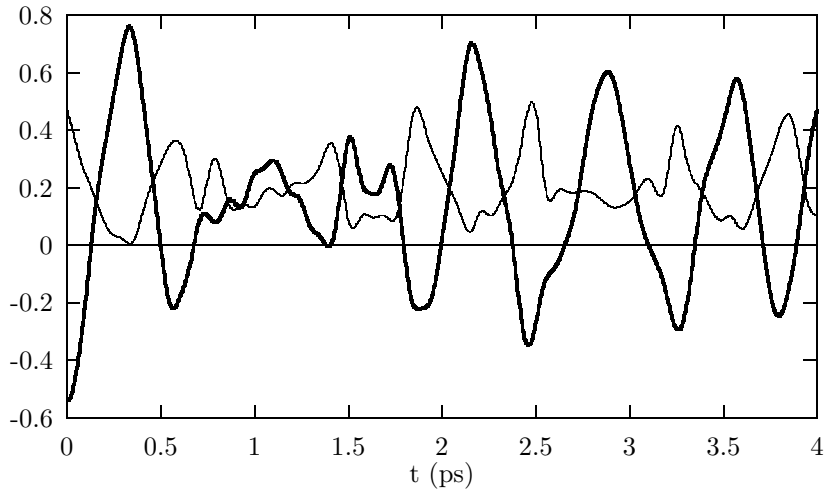


Figure 6b. Thick curve shows the site population difference obtained with same system parameters and excitation conditions as in the lower (thin) curve of Fig. 1. The corresponding anisotropy is shown with a thin curve.

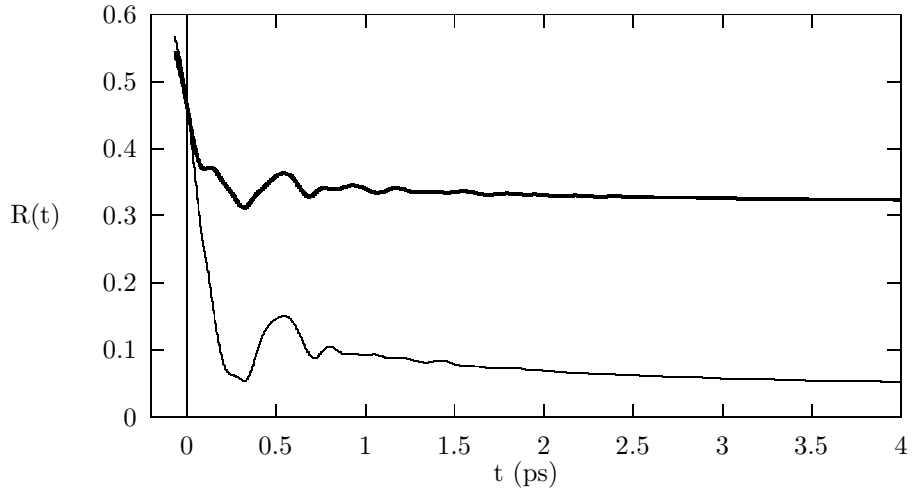


Figure 7. Time-resolved anisotropy for chromophore pair with same parameters as in Figure 1 and a  $1.5 \text{ ps}^{-1}$  vibrational relaxation rate. Upper (thick) curve is for excitation at zero-zero transition frequency of lower-energy chromophore, lower (thin) curve is for excitation  $100 \text{ cm}^{-1}$  above the zero-zero transition frequency of the higher energy chromophore. The vibrational and electronic ground state of the chromophore pair is the only initial state included.

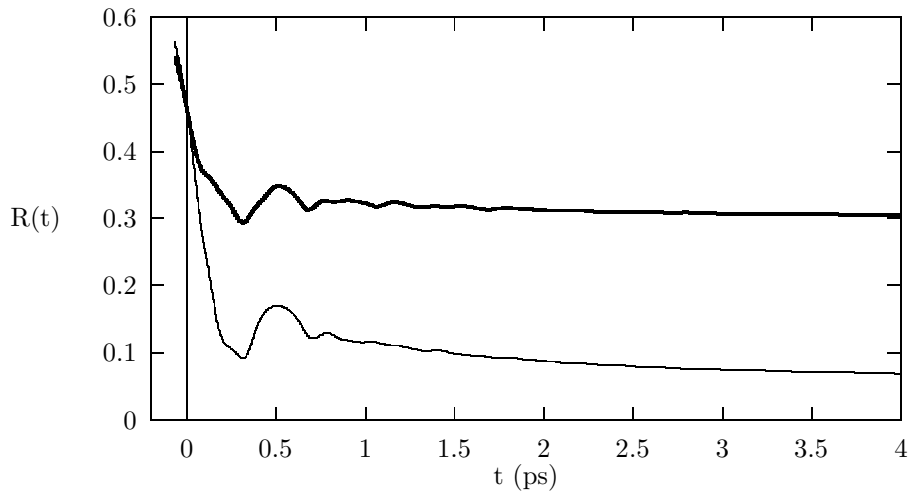


Figure 8. Time-resolved anisotropy for chromophore pair with the same parameters as in Figure 1 and a  $1.5 \text{ ps}^{-1}$  vibrational relaxation rate. Three lowest thermally populated initial states have been included.

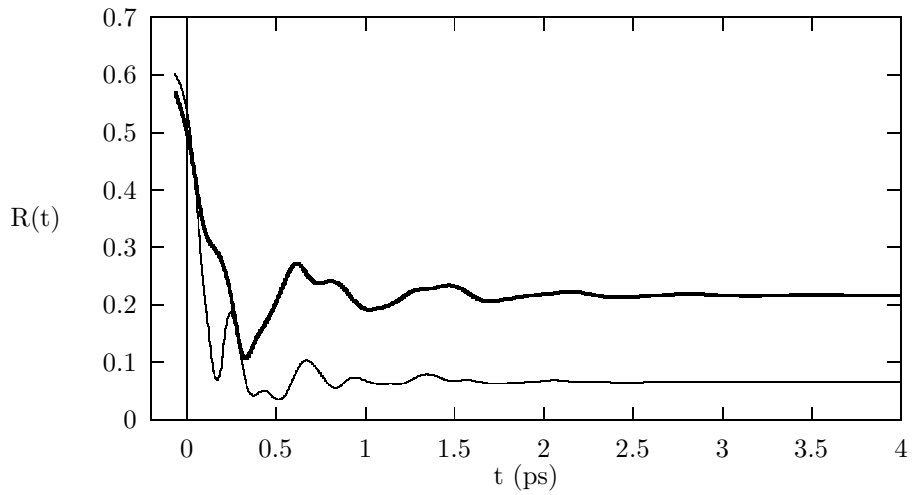


Figure 9. Time-resolved anisotropy for pair of identical chromophores with the same parameters as in Figure 4 and a  $1.5 \text{ ps}^{-1}$  vibrational relaxation rate. Upper (thick) curve corresponds to excitation at zero-zero transition frequency of either chromophore, lower (thin) curve is for excitation  $250 \text{ cm}^{-1}$  above the zero-zero transition frequency of either chromophore.

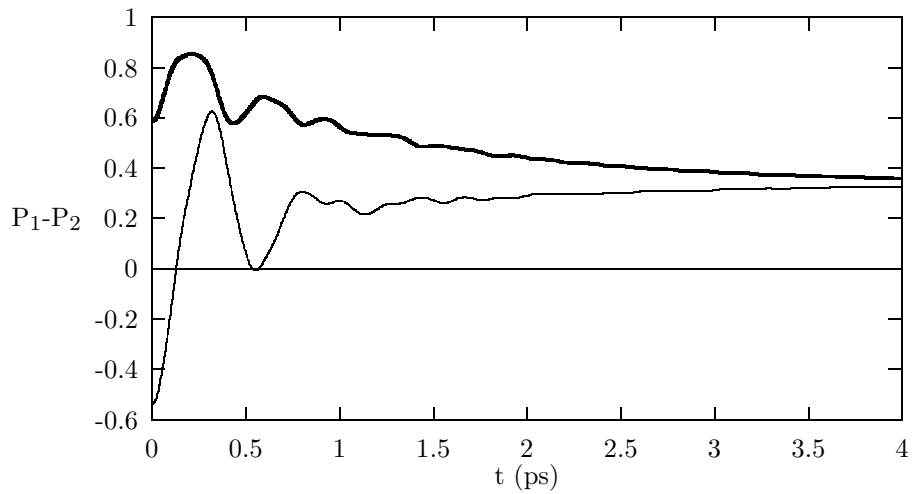


Figure 10. Site population difference for the chromophore pair with  $150\text{ cm}^{-1}$  offset between the zero-zero electronic transition frequencies and a  $1.5\text{ ps}^{-1}$  vibrational relaxation rate. Upper (thick) curve is for excitation at zero-zero transition frequency of lower-energy chromophore, lower (thin) curve corresponds to excitation  $100\text{ cm}^{-1}$  above the zero-zero transition frequency of higher-energy chromophore.